535.36

OPTICAL PROPERTIES OF POLYVALENT NON-TRANSITION METALS

G. P. MOTULEVICH

P. N. Lebedev Physics Institute, USSR Academy of Sciences

Usp. Fiz. Nauk 97, 211–256 (February 1969)

INTRODUCTION

IN this review, we shall attempt to present a picture of the metal-optical phenomena, brought in correspondence with the modern state of solid state physics, and to demonstrate the great capabilities of metal optics, which makes it possible to obtain extensive information concerning the electron structure of metals.

Analysis of the status of this branch of physics, as of the end of 1955, is presented in a review by Ginzburg and the author.[1] At that time, an important step that stimulated the development of metal-optical research was the application to optics (principally to the infrared region of the spectrum) in 1953–1954, by Dingle[2] and Ginzburg[3], of the theory of the anomalous skin effect, previously developed by Pippard,[4] Reuter and Sondheimer,[5] Chambers,[6] Holstein[7] and others for measurements in the microwave band. This theory eliminated the contradiction between the experimental and theoretical values of the light absorption coefficient A at low temperatures. Experiment shows that with lowering temperature the indicated coefficient remains quite large (see the review [1]) whereas, according to earlier theories by Drude and Zener,[8] it should tend to zero. According to the theory of the anomalous skin effect, it is necessary to take into account the contribution made to A by surface losses, which remain finite also at T = 0 in the case of diffuse reflection of the electrons from the surface of the metal.* Allowance for this circumstance, and also allowance for the quantum character of the interaction between the electron with the photon and the phonons, as presented in 1954–1958 by Gurzhi[10,11] and Holstein,[12] has led to agreement between the experimental and theoretical temperature dependences of A.

The review [1] presents a theory relating the optical constants of metals with their microscopic characteristics, based on the isotropic model of "almost free" electrons, with account taken of the anomalous character of the skin effect. It also emphasizes the importance of metal-optical measurements, particularly measurements in the infrared region, which make it possible to determine the concentration of the conduction electrons. An analysis was performed of the experimental papers, indicating that no reliable data on the optical constants of metals, particularly in the infrared region, were available at that time. Moreover, for the infrared region there were no methods that made it possible to perform measurements with good accuracy. Methods of preparing samples for the investigation suffered from major defects.

During the elapsed time, new methods were developed for the measurement of optical constants of metals, and the problem of obtaining samples of the required quality was solved. As a result, reliable data were obtained on the optical constants of a number of metals.

Appreciable progress was made also in the theoretical analysis of the connection between the optical properties of metals and their basic microscopic characteristics. The development of solid-state theory has led recently to very fruitful ideas, connected with the concept of pseudopotential. These ideas were developed by Harrison,[13] Heine,[14,15] Ziman[16–19] and a number of other authors. According to these papers, the screening of the ion by electrons, and also the possibility of using the smoothing of rapid oscillations of the electron within the ionic residue, make it possible to work with a pseudowave function and a pseudopotential. The pseudopotential is in essence the difference between the screened potential of the ion and the effective potential connected with the rapid oscillatory motion of the electron inside the ion. It is much smaller than the initial potential and represents a much smoother function than the true potential. The pseudowave function corresponds to the true wave function without allowance for the rapid oscillations inside the ionic residue.

It became clear after the publication of the aforementioned papers that it is possible to assume in practice for many problems that the valence electron "feels" only the weak pseudopotential. This justifies the model of the "almost free" electrons and makes it possible to consider the optical properties of ordinary metals in the infrared and in the visible regions of the spectrum also on the basis of the concept of the "almost free" electrons. But the properties of these "almost free" electrons differ from the properties of "free" electrons.

Coherent scattering of electrons by the lattice planes, even in the case of a weak pseudopotential, greatly affects the optical properties of the metals.

Using the concept of the pseudopotential, it was possible to obtain simple relations between the optical constants of the metal and its basic electronic characteristics. Thus, measurement results made it possible to determine the main characteristics of the conduction electrons and the Fourier components of the pseudopotential. Since the same microscopic characteristics, and primarily the Fourier components of the pseudopotential, determine both the band structure and other properties that depend on the electron-ion interaction (for example, the van Alphen–de Haas effect, cyclotron resonance, the phonon spectrum and absorption of ultrasound in a magnetic field, the temperature of the transition to the superconducting state, etc.), it is possible to use optically-obtained data to interpret other data.

The approach considered in the present paper can be extended not only to metals in the crystalline state, but

*The diffuse reflection of electrons from metal surfaces has been confirmed by experiment [6,9].

also to liquid metals, to alloys (both ordered and disordered), and to the amorphous state of metals.

The presented relations hold for ordinary, i.e., non-transition metals. It is not clear as yet to what extent they can be transferred to transition metals. We shall henceforth consider only non-transition metals.

A more detailed analysis of all the questions touched upon in the present review can be found in [20].

1. THE KINETIC-EQUATION METHOD IN METAL OPTICS

Optical measurements make it possible to obtain two functions $n(\omega, T)$ and $\kappa(\omega, T)$ (see [1]).* To establish the connection between $n(\omega, T)$ and $\kappa(\omega, T)$, on the one hand, and the basic electronic characteristics of the metal on the other, one uses the method of the kinetic equation (see, for example [21,22,1]). The state of the electrons is described by a distribution function $\tilde{f}(\mathbf{p}, \mathbf{r}, t)$ that depends on the indicated arguments.† It satisfies the following relation:

$$\tilde{f}(\mathbf{p}, \mathbf{r}, t) = f_0(\mathbf{p}) + f(\mathbf{p}, \mathbf{r}, t), \tag{1.1}$$

$$f_0(\mathbf{p}) = \left[\exp\left(\frac{E-E_F}{kT}\right) + 1\right]^{-1}, \tag{1.2}$$

and $f(\mathbf{p}, \mathbf{r}, t)$ is determined by the influence of the field of the light wave. In all cases encountered at the present time in metal optics it can be assumed that $|f| \ll |f_0|$. We can therefore use a linearized kinetic equation that should be solved simultaneously with the field equations. The complete system of equations, written out for the case when the metal occupies the upper half-space, the z axis is perpendicular to the interface, and light of frequency ω, polarized along the x axis, is incident on the metal normally to the surface, has the following form:

$$v_z \frac{\partial f}{\partial z} + (i\omega + \nu) f = -e\mathscr{E}_x \frac{\partial f_0}{\partial p_x}, \tag{1.3}$$

$$\frac{d^2\mathscr{E}_x}{dz^2} + \frac{\omega^2}{c^2}\mathscr{E}_x = i \cdot \frac{4\pi\omega}{c^2} j_x, \tag{1.4}$$

$$j_x = \frac{2e}{(2\pi\hbar)^3}\int v_x f\, d^3p. \tag{1.5}$$

We assume that $\mathscr{E}$ coincides with the direction of $\mathbf{j}$ (isotropic case or polycrystal). In Eq. (1.3), account is taken of the fact that $\partial f/\partial t = i\omega f$, and the collision integral is written in the form $-\nu f$. Such an approximate notation, when account is taken of only the first term of the expansion of the collision integral in powers of f, is justified at high (room) temperatures, and also at low (helium) temperatures.[22-24,10] This approximation can also be used as an extrapolation at medium temperatures.

Equation (1.3) is classical. At high frequencies, however, when $\hbar\omega > kT$, the interaction of the electrons with the field of the light wave has a quantum character. The electron, absorbing a quantum of light, changes its energy immediately by an amount $\hbar\omega$. The difference between the classical and quantum cases is particularly significant when the following inequalities are satisfied: $\hbar\omega \gg k\Theta \gg kT$ (here Θ is the Debye temperature), i.e., in low-temperature measurements. It is more correct to use the quantum kinetic equation. Gurzhi, developing work by Bogolyubov and Gurov[25] and Klimontovich and Silin,[26] obtained a quantum kinetic equation for electrons in a metal in the field of an electromagnetic wave.[10,11] As the quantum distribution function, one takes the mixed representation of the density matrix. The equation obtained for this function contains a certain operator, which is a quantum generalization of the usual collision integral. We shall not present here the complicated expressions for this operator. We note only that for metal-optical problems, in the case when the inequalities

$$\exp\left(\frac{\hbar\omega}{kT}\right) \gg 1 \text{ and } \exp\left(\frac{\hbar\omega}{kT}\right) \gg \exp\left(\frac{\Theta}{T}\right)$$

are satisfied, it is possible to introduce the effective electron-phonon collision frequency $\nu_{ep}(T)$ which, however, differs greatly at low temperatures from the classical electron-phonon collision frequency $\nu_{ep}^{cl}(T)$. This difference will be discussed in greater detail in Ch. 6.

The effective electron collision frequency, generally speaking, can receive contributions also from interelectron collisions. The influence of the interelectron interaction on this quantity is considered in works by Ginzburg and Silin,[27] Pitaevskiĭ,[28] and Gurzhi.[29] The interelectron interaction in metals is strongly suppressed by the Pauli principle. An electron lying in the Fermi smearing zone may collide only with another electron from the same region. After collision, both electrons should again fall somehow into the Fermi smearing zone. It is possible to take all these collisions into account by introducing an additional frequency ν_{ee}, which leads to additional absorption of light. According to [28],

$$\nu_{ee}(\omega, T) = \nu_{ee}^{\text{кл}}(T)\left[1 + \left(\frac{\hbar\omega}{2\pi kT}\right)^2\right]; \tag{1.6}$$

Here ν_{ee}^{cl} is the corresponding classical frequency of the interelectron collisions, which is proportional to T^2. In the near infrared $\hbar\omega \gg 2\pi kT$ and $\nu_{ee} \gg \nu_{ee}^{cl}$. Thus, observation of the frequency of the interelectron collisions is much more probable in optics than in statics. However, experimental investigations of the optical constants of metals, performed in a wide range of temperatures, have shown that even in optics we have $\nu_{ee} \ll \nu$ and it can be observed only at helium temperatures in metals in which there are no interband transitions in the near infrared region.[30-32]

Finally, we note that scattering of electrons by impurities (by impurities we mean both chemical impurities and physical impurities, i.e., scattering by inhomogeneities, crystal boundaries, etc.) can be taken into account by introducing the frequency ν_{ed} of the collisions with impurities.

Thus, we get for ν the following expression:

$$\nu = \nu_{ep} + \nu_{ee} + \nu_{ed}. \tag{1.7}$$

Returning to Eq. (1.3), we note that

$$\frac{\partial f_0}{\partial p_x} = v_x \frac{\partial f_0}{\partial E}.$$

The function $\partial f_0/\partial E$ has a δ-like character, as a result

*A list of the symbols employed in this paper is given at the end of the review on p. 102.

†The spin variables can be disregarded.

of which the optical properties are determined by the electrons on the Fermi surface.

The magnitude of the first term of Eq. (1.3) $v_z\,\partial f/\partial z$ determines the character of the skin effect. If this term can be neglected, then we have the so-called normal skin effect, which is realized primarily for liquid metals and metals in the amorphous state. It also takes place for certain metals in the crystalline state, in the visible section of the spectrum, and in the near infrared region at high (room) temperatures.

If $v_z\,\partial f/\partial z \gg (i\omega+\nu)f$, then the sharply anomalous skin effect takes place. This case is realized for crystalline metals in the microwave band. In the infrared region, it occurs only for metals of the first group at low (helium) temperatures.

If the term $v_z\,\partial f/\partial z$ is small, but must still be taken into account as a correction, then we deal with the weakly-anomalous skin effect. This is the most widespread case for metals in the crystalline state in the infrared region of the spectrum. For polyvalent metals, it occurs at all temperatures. For monovalent metals it takes place at high (room) temperatures.

We shall dwell below only briefly on the features of the general solution of the system of equations (1.3)–(1.5), paying particular attention to the cases of practical importance, namely the weakly-anomalous and normal skin effects.

a) Anomalous Skin Effect

The general solution of Eqs. (1.3)–(1.5) has been considered in a number of papers.[1-3,5,33-35] In all the papers they considered only a spherical Fermi surface. In the general case, a nonlocal connection is produced between the current density and the polarization inside the metal and the electric field of the light wave. It is then impossible to introduce a complex dielectric constant ϵ'. However, it is possible here, too, to use the surface impedance Z and to relate to it the magnitude of the effective complex dielectric constant $\epsilon'_{\text{eff}} = (n_{\text{eff}} - i\kappa_{\text{eff}})^2$. Usually $1/|\epsilon'_{\text{eff}}| \ll 1$; then*

$$Z = \frac{4\pi}{c\sqrt{\varepsilon'_{\text{eff}}}}. \tag{1.8}$$

The surface impedance characterizes completely the reflection of the electromagnetic waves from the metallic surface. The connection between the surface impedance and the boundary conditions is analyzed in [37] and is presented in [1]. Experiment makes it possible to determine n_{eff} and κ_{eff}, using the properties of the reflected light in the same manner as n and κ are determined. We shall henceforth omit the subscript "eff."

Let us return to the solution of the system of Eqs. (1.3)–(1.5). The solution of this system depends significantly on the character of the reflection of the electrons from the surface of the metal. The experiment has shown that if we are not interested in extremely oblique incidence of the electrons on the surface of the metal, then the reflection is diffuse both in the case of polycrystals and in the case of single crystals.[6,9] Without stopping to discuss these methods, which were specially developed for the solution of this system of equations, we shall indicate that in place of the ordinary Ohm's law there exists in this case between the current density and the field an integral relation of the type

$$j(z) = \int_0^\infty K\left(\frac{z-\xi}{l}\right)\mathscr{E}(\xi)\,d\xi;$$

The kernel K differs significantly from zero if the argument is ≤ 1. Such a connection between the current and the field leads to an integro-differential equation for the field in the metal, of the type

$$\frac{d^2\mathscr{E}}{dz^2} + \frac{\omega^2}{c^2}\mathscr{E} = \text{const}\cdot\int_0^\infty K\left(\frac{z-\xi}{l}\right)\mathscr{E}(\xi)\,d\xi.$$

Its solution is complicated and cumbersome. The final results are obtained only after numerical integration. The decrease of the field $\mathscr{E}$ with increasing depth remains very rapid, although not exponential.

Usually one obtains expressions for the real and imaginary parts of the surface impedance Z in the form of expansions in small parameters. We have already mentioned that the anomalous skin effect is realized in optics only for metals of the first group at low temperatures. In this case the inequality $\nu/\omega \ll 1$ is satisfied. Therefore one uses as one of the parameters of the expansion the ratio ν/ω. The second parameter is usually the quantity $v_F/\omega\delta$. The smallness of this parameter signifies that the path traversed by the electron in one period is small compared with the depth of the skin layer. The expressions for the real and imaginary parts of the surface impedance in the case of the anomalous skin effect are given in [1-3,38]

b) Normal Skin Effect

The normal skin effect has been discussed in many papers, and particularly in the review.[1] It corresponds to neglect of the first term in Eq. (1.3), after which the equation changes from differential to algebraic. Under this condition, the reflections of the electrons from the boundary of the metal are insignificant, and all the optical constants are determined by volume effects.

The normal skin effect can be readily analyzed for a single crystal with an arbitrary Fermi surface. We choose the axes x, y, and z along the principal axes of the ϵ' ellipsoid. Then, for the experimental setup indicated at the beginning of this section (z axis perpendicular to the surface of the metal, field polarized along the x axis), we have $\mathscr{E} \uparrow\uparrow j$. We determine f(z) from (1.3), substitute it in (1.5), and after changing over from the volume integral to an integral over the Fermi surface, we obtain

$$j_x(z) = \frac{i\omega}{4\pi}(\varepsilon_x'^{\text{n}} - 1)\mathscr{E}_x(z) = \frac{2e^2}{(2\pi\hbar)^3}\frac{\mathscr{E}_x(z)}{i\omega+\nu_x}\oint\frac{v_x^2}{v}\,dS_F;$$

here dS_F is an element of the Fermi surface; the index "n" denotes that the corresponding quantity pertains to the normal skin effect. We have taken the quantity $1/(i\omega+\nu)$ outside the integral sign, i.e., we have used the theorem of the mean, and marked ν with the index x. Similar relations can be obtained for $j_y(z)$ and $j_z(z)$. Thus, we obtain the following formulas for the compo-

*Allowance for the corrections connected with the terms $\sin^2\varphi/\epsilon'$ entails no difficulties. The corresponding corrections for n_{eff} and κ_{eff} were considered, for example, in [36]; they are given in Ch. 3 of the article.

nents of the complex dielectric constant:

$$\varepsilon_i'^{n} - 1 = -\frac{4\pi e^2}{\omega(\omega - i\nu)}\left(\frac{N}{m}\right)_i, \tag{1.9}$$

$$\left(\frac{N}{m}\right)_i = \frac{2}{(2\pi\hbar)^3}\oint \frac{v_i^2}{v}\, ds_F \qquad (i = x,\ y,\ z). \tag{1.10}$$

Determining experimentally the free complex quantities $\epsilon_x'^{n}$, $\epsilon_y'^{n}$, and $\epsilon_z'^{n}$ we can determine the six quantities

$$(N/m)_i \text{ и } \nu_i\ (i = x,\ y,\ z).$$

For metals of the cubic system we have

$$\oint \frac{v_x^2}{v}\, ds_F = \oint \frac{v_y^2}{v}\, ds_F = \oint \frac{v_z^2}{v}\, ds_F = \frac{1}{3}\oint v\, ds_F, \qquad \nu_x = \nu_y = \nu_z = \nu,$$

and formulas (1.9) and (1.10) simplify:

$$\varepsilon'^{n} - 1 = -\frac{4\pi e^2}{\omega(\omega - i\nu)}\frac{N}{m}, \tag{1.9a}$$

$$\frac{N}{m} = \frac{2}{3(2\pi\hbar)^3}\oint v\, ds_F. \tag{1.10a}$$

Expression (1.9a) has the same form as for a free classical electron gas with a conduction-electron density N and with mass m equal to the mass of the free electron.* In just this sense, we shall call the quantity N, defined by formula (1.10a), the density of the conduction electrons.†

It is easy to estimate the magnitude of the discarded terms. To this end, we substitute ϵ_n' from (1.9a) into (1.4). We then substitute the solution for the field $\mathscr{E}$ in (1.3), after which we obtain the following conditions under which we can neglect the term $v_z\, \partial f/\partial z$ (see the review [1]):

$$\frac{n_n v_F}{c} \ll 1, \tag{1.11a}$$

$$\frac{\varkappa_n v_F}{c} \ll \frac{\nu}{\omega} \quad \text{or} \quad l \ll \delta. \tag{1.11b}$$

The inequality (1.11a) is satisfied for all the metals. The inequality (1.11b) is by far not always satisfied.

The review [1] contains formulas obtained for the optical constants of metals by series expansion in the parameters ν/ω and $v_F/\omega\delta$. These formulas do not hold in the case when ν is of the order of ω. To determine N and ν from the experimental data it is convenient in this case to use the following relation:[30,40]

$$(\varepsilon_n' - 1)^{-1} = -\frac{\omega(\omega - i\nu)}{4\pi e^2}\frac{m}{N}. \tag{1.12}$$

c) Weakly Anomalous Skin Effect

Experimental investigations have shown that the weakly anomalous skin effect is the most widespread for metals in the crystalline state. It was considered in detail in [41,20]. Unlike the general case, where there are solutions either for $\nu \ll \omega$ or for $\nu \gg \omega$, for the weakly-anomalous skin effect there were obtained analytic solutions that are valid for any relation between ν and ω.

The solution of the system (1.3)–(1.5) for this case is obtained by successive approximations. The problem has a small parameter equal to

$$\frac{3}{8}\frac{v_F}{c}\frac{n - i\varkappa}{1 - i(\nu/\omega)}.$$

We shall assume, as before, that the field $\mathscr{E}$ in the metal coincides in direction with j (isotropic case or polycrystals).* In the zeroth approximation, we neglect in (1.3) the term $v_z\, \partial f/\partial z$, after which we obtain the normal skin effect considered above. The solution for the field in the zeroth approximation will be substituted in the right side of Eq. (1.3). We obtain the first-approximation equation

$$v_z\frac{\partial f}{\partial z} + (i\omega + \nu) f = -\frac{\partial f_0}{\partial E}\frac{v_x}{v_z} e\mathscr{E}(0) \exp\left[-i\frac{\omega}{c}(n_n - i\varkappa_n)\right]; \tag{1.3a}$$

Here $\mathscr{E}(0)$ is the field on the surface of the metal. As boundary conditions we use the conditions corresponding to the diffuse reflection of the electrons from the surface of the metal:

$$\begin{cases} \text{for } v_z > 0\ f = 0 \quad \text{if} \quad z = 0 \text{ and } f = 0 \quad \text{as} \quad z \to \infty; \\ \text{for } v_z < 0 \qquad\qquad\qquad\qquad f = 0 \quad \text{as} \quad z \to \infty. \end{cases}$$

Substituting the solution of (1.3a) in (1.5), we obtain

$$j_x(z) = \frac{2e^2\mathscr{E}_x(0)}{(2\pi\hbar)^3}\oint \frac{\exp\left[-i\frac{\omega}{c}(n_n - i\varkappa_n) z\right] - B\exp\left(-\frac{i\omega + \nu}{v_z} z\right)}{\frac{i\omega + \nu}{v_z} - i\frac{\omega}{c}(n_n - i\varkappa_n)}\frac{v_x^2}{v_z}\frac{dS_F}{v}. \tag{1.13}$$

B = 1 for $v_z > 0$ and B = 0 for $v_z < 0$. Equation (1.13) shows that there is no local connection between $j_x(z)$ and $\mathscr{E}_x(z)$. We calculate next the total current

$$I_x = \int_0^\infty j_x(z)\, dz,$$

and the surface impedance† $Z = I_x/\mathscr{E}_x(0)$. Using the central symmetry of the Fermi surface and confining ourselves to terms of first order in $(v/c)(n - i\kappa)/[1 - i(\gamma/\omega)]$, we obtain

$$(Z)^{-1} = (Z_n)^{-1}(1 - \alpha), \tag{1.14}$$

$$(Z_n)^{-1} = -\frac{2e^2}{(2\pi\hbar)^3}\frac{c}{\omega(\omega - i\nu)(n - i\varkappa)}\oint \frac{v_x^2}{v}\, dS_F, \tag{1.15}$$

---

*Vonsovskiĭ [39] has shown that a connection between the dielectric constant and the conduction-electron density, similar to (1.9a) can also be obtained by a quantum method, using the density matrix.

† One sometimes uses in lieu of N and m the quantities N_{val} and m_{eff}, defined by the relation $N/m = N_{val}/m_{eff}$. Since we can determine from experiment only the ratio N/m, the two approaches are equivalent. We shall use the quantity N.

*Kaganov and Slezov [42] considered the case of arbitrary anisotropy. They were interested, however, only in the region $\nu \ll \omega$.

† For cubic symmetry and arbitrary orientation of the crystal, the direction of j coincides in the zeroth approximation with the direction of $\mathscr{E}$. In the first approximation, in the presence of a field $\mathscr{E}_x$, both j_x and j_y differ from zero. With the same degree of accuracy, we obtain

$$\frac{I_y}{I_x^0} = \frac{i\omega}{c}\frac{n - i\varkappa}{i\omega + \nu}\frac{\oint'_{v_z > 0} v_x v_y v_z\, dS_F/v}{\oint v_x^2\, dS_F/v};$$

Here I_y is the total current along the y axis; I_x^0 is the total current along the x axis in the zeroth approximation. At an arbitrary orientation of the crystal we have $|I_y/I_x^0| < |\alpha|$. The presence of I_y leads to the appearance of nondiagonal terms Z_{xy} and ϵ_{xy}. These terms, however, are small and they can be neglected in practice. Thus, the obtained formulas can be used in practice also for cubic single crystals. In the isotropic case or in the case when the fourfold symmetry axes are parallel to the axes x and z we have $I_y = Z_{xy} = \epsilon'_{xy} = 0$.

$$\alpha = \frac{1}{c}\frac{n-i\varkappa}{1-i\frac{\nu}{\omega}}\frac{\oint'_{v_z>0} v_x^2 v_z\, dS_F/v}{\oint v_x^2\, dS_F/v}; \qquad (1.16)$$

here Z_n is the surface impedance for the normal skin effect, $\int'_{v_z>0}(\ldots)dS_F$ is an integral over the part of the Fermi surface for which $v_z > 0$. Using (1.8), obtain

$$(\varepsilon')^{-1}(1-2\alpha) = (\varepsilon^{n'})^{-1}, \qquad (1.17)$$

where $\epsilon^{n'}$ is given by formula (1.9a). The small correction term α can be calculated with lower accuracy and one can use the expression obtained for the isotropic case:

$$2\alpha = \frac{3}{8}\frac{v_F}{c}\varkappa\frac{1+i(n/\varkappa)}{(\nu/\omega)+i}. \qquad (1.18)$$

Formulas (1.17), (1.9a), (1.10a), and (1.18) give the connection between the optimal constants of the metals and N and ν.

The complex expansion parameter used for the weakly-anomalous skin effect is a combination of several dimensionless ratios, namely

$$\frac{3}{8}\frac{v_F}{c}\frac{n-i\varkappa}{1-i\nu/\omega} = \frac{3}{8}\frac{[n(v_F/c)+(l_1/2\pi\delta)(\nu/\omega)]+i[n(v_F/c)(\nu/\omega)-l_1/(2\pi\delta)]}{1+\nu^2/\omega^2};$$

Here $l_1 = 2\pi v_F/\omega$ is the path traversed by the electron during the period of the field. After performing the experiment, it is always possible to calculate the value of this complex parameter and to establish the character of the skin effect.

In concluding this chapter, we note that the optical measurements in the infrared region make it always possible, i.e., for any character of the skin effect, to determine the quantity

$$\frac{N}{m} = \frac{2}{3(2\pi\hbar)^3}\oint v_F dS_F.$$

2. INFLUENCE OF PERIODIC LATTICE POTENTIAL ON THE OPTICAL PROPERTIES OF METALS*

The periodic lattice potential has a strong influence on the optical properties of metals in both the visible and infrared regions of the spectrum. In determining the influence of the periodic potential of the lattice, we use the concept of the pseudopotential, mentioned in the introduction. We expand the pseudopotential in a Fourier series:

$$V(\mathbf{r}) = \sum_{\mathbf{g}} V_{\mathbf{g}} \exp(2\pi i \mathbf{g}\mathbf{r}). \qquad (2.1)$$

The summation is over all the reciprocal-lattice vectors **g**. The sign of the vector in the index **g** will be henceforth omitted. The experimental determinations of V_g, performed both by the optical method[20,46-50] and by the method of investigating the van Alphen–de Haas effect,[51,52] show that the following inequalities are satisfied for metals:

$$\frac{|V_g|}{E_F} \ll 1. \qquad (2.2)$$

This makes it possible to use the weak-coupling approximation, considered in detail in many papers, particularly in [16,19,53].

The effects which we shall consider are the differences between N and N_{val}, S_F^0 and S_F, and $\langle v_F\rangle$ and v_F^0; all these differences are of the order of unity. Therefore to determine the main features of the phenomenon it suffices to take into account the terms of first order in $|V_g|/E_F$. This makes it possible to obtain simple analytic expressions that determine the deviations of the basic electronic characteristics N, S_F, and $\langle v_F\rangle$ from the corresponding characteristics of free electrons. In this approximation, the action of the sum of the Fourier components of V_g is equal to the sum of the action of each component. To each periodic potential in coordinate space, described by a term of the sum (2.1), there corresponds in momentum space a separate Bragg plane, the equation of which is

$$\mathbf{p}_g(\mathbf{p}-\mathbf{p}_g) = 0; \qquad (2.3)$$

Here $2\mathbf{p}_g = 2\pi\hbar\mathbf{g}$, $p_g = |\mathbf{p}_g|$ is the distance from the center of the band Γ to the Bragg plane. As already indicated, in our approximation the action of the sum of the Bragg planes is equal to the sum of the actions of each Bragg plane.

Let us consider the action of one Bragg plane. Figure 1 shows the sphere of free electrons for a concentration equal to the valence concentration. The plane (p_y, p_z) passing through the point 0 is the Bragg plane that intersects the sphere of the free electrons. The deviation of the motion of the electron from the free motion is principally connected with the coherent scattering by the lattice planes. This is realized only in the case when the momentum of the electron is close to the Bragg plane. Therefore, everywhere away from the Bragg plane, the Fermi surface will coincide with the sphere of the free electrons. Near the intersection of the Bragg plane with the sphere of the free electrons, the Fermi surface assumes the form shown in Fig. 1. It is a surface of revolution with a symmetry axis perpendicular to the Bragg plane. Thus, the Bragg plane changes the shape of the Fermi surface and its magnitude.

A similar conclusion can be drawn with respect to the velocity of the electron on the Fermi surface, v_F. Far from the Bragg plane we have $v_F \approx v_F^0$. Near the Bragg plane $v_F < v_F^0$.

The ring M_1M_2 on the Bragg plane (Fig. 2) between the two circles obtained when the Bragg plane intersects the Fermi surface, are not part of the Fermi surface, since the energy of the electrons whose state is repre-

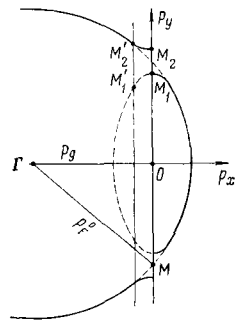

FIG. 1. Intersection of the free-electron sphere and one Bragg plane. The Bragg plane coincides with the plane (p_y, p_z); $\Gamma M = p_F^0$; $\Gamma O = p_g$. The zone with the higher number in the band scheme is shown dashed. The plane $M'_2M'_1$ is parallel to the Bragg plane.

*The questions of this chapter are discussed in greater detail in [20, 43–46].

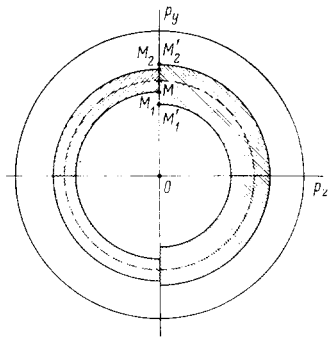

FIG. 2. Intersection of the Fermi surface with the Bragg plane and with a plane parallel to the Bragg plane. On the left is shown the ring M_1M_2 on the Bragg plane; on the right is shown the ring $M'_1M'_2$ on a plane parallel to the Bragg plane.

sented by the points of this ring is not equal to E_F. The wave function of the electron far from the Bragg plane can be regarded as a plane wave, and that near the Bragg plane can be regarded as a sum of two plane waves.

a) Long Wave Region

We proceed to consider the influence of the periodic potential of the lattice on the optical constants in the long-wave region. By long-wave region we mean the region in which the influence of the interband transitions on the optical constants can be neglected. Each metal has its own boundary of the long-wave region. However, for a large group of non-transition metals, it is possible to assume that the long-wave region is $\lambda > 2-3\,\mu$. The optical properties of the metals are determined here by the conduction electrons, i.e., by the electrons on the Fermi surface. We shall use the scheme of expanded bands.

We need to determine the influence of V_g on S_F, $\langle v_F \rangle$, and $\langle v_F \rangle S_F$. In our approximation, the electron energy is determined from the second-order secular equation (see, for example, [16,19,53]). Introducing the dimensionless quantities

$$x = \frac{p_\perp - p_g}{p_g}, \quad y = \frac{p_\parallel}{p_g}, \tag{2.4}$$

$$w = \frac{2mE}{p_g^2}, \quad \xi = \frac{2m\,|V_g|}{p_g^2} \tag{2.5}$$

($p_\perp$ and $p_\parallel$ are the momentum components perpendicular and parallel to the Bragg plane), we obtain the equation of the equal-energy surface in the form

$$w = 1 + x^2 + y^2 + \operatorname{sign}(x)\sqrt{4x^2+\xi^2}. \tag{2.6}$$

On the Bragg plane $x = 0$ and $w = w_0 \pm \xi$, i.e., $E = E_0 \pm |V_g|$ (the index "0" denotes that the corresponding quantity pertains to the free electrons). Near the Bragg plane, when $4x^2 \ll \xi^2$, the energy corrections are of first order, $\sim |V_g|$, and far from the Bragg plane they are of second order.

Equation (2.6) makes it possible to determine the influence of the Bragg plane on the electron velocity. This plane does not change the velocity component parallel to it, i.e., $v_\parallel = \partial E/\partial p_\parallel = v_\parallel^0$. The velocity component perpendicular to the plane, $v_\perp = \partial E/\partial p_\perp$, does change. In terms of the variables (2.4) and (2.5), we have

$$v_\parallel = \frac{p_g}{m}\,y, \tag{2.7}$$

$$v_\perp = \frac{p_g}{m}\left[x + \operatorname{sign} x \frac{2x}{\sqrt{4x^2+\xi^2}}\right], \tag{2.8}$$

$$v^2 = v_\parallel^2 + v_\perp^2 = \frac{p_g^2}{m^2}\left[w - \frac{\xi^2}{4x^2+\xi^2} - \operatorname{sign} x \frac{\xi^2}{\sqrt{4x^2+\xi^2}}\right]. \tag{2.9}$$

We have already indicated that as a result of the action of one Bragg plane the equal-energy surface is a surface of revolution. The area element of the equal-energy surface is

$$dS = 2\pi p_g^2 y(x)\sqrt{1+[y'(x)]^2}\,dx,$$

where y(x) is determined by Eq. (2.6) at w = const; hence

$$dS = 2\pi m p_g v\,dx. \tag{2.10}$$

For the Fermi surface

$$dS_F = 2\pi m p_g v_F\,dx. \tag{2.10a}$$

It is easy to show that the change of the Fermi surface considered above leads to a change in the volume of the momentum space lying inside this surface, determined by quantities of second order of smallness. This means that, with our accuracy, $E_F = E_F^0$ and that far from the Bragg surface $p_F = p_F^0$.

Let us use the obtained expressions to determine the electronic characteristics of interest to us. We consider first N. According to (1.10a) and (2.10a)

$$N \sim \oint v_F\,dS_F \sim \int v_F^2\,dx;$$

Therefore

$$\frac{N_{\text{val}} - N}{N_{\text{val}}} \equiv \frac{v_F^0 S_F^0 - \langle v_F \rangle S_F}{v_F^0 S_F^0}. \tag{2.11}$$

The limits of integrations are

$$x_g = \frac{p_F}{p_g} - 1 \quad \text{и} \quad x'_g = -\frac{p_F}{p_g} - 1. \tag{2.11a}$$

Using (2.9) and (2.10a), and taking into account the action of all the Bragg planes, we obtain

$$\frac{N_{\text{val}} - N}{N_{\text{val}}} = \sum_g \frac{\pi}{4}\frac{p_g}{p_F^0}\frac{|V_g|}{E_F^0}\left(\frac{1}{2} + \frac{\varphi_g}{\pi}\right), \tag{2.12}$$

$$\varphi_g = \operatorname{arctg}\frac{2\,(p_g/p_F^0)\,(1 - p_g/p_F^0)}{|V_g|/E_F^0}. \tag{2.12a}$$

The summation is over all the Bragg planes intersecting the sphere of the free electrons. We note that when the inequality $x_g \gg \xi/2$ is satisfied, meaning that

$$\frac{p_F^0 - p_g}{p_g} \gg \frac{1}{2}\frac{|V_g|}{E_F^0}\left(\frac{p_F^0}{p_g}\right)^2,$$

we get

$$\frac{1}{2} + \frac{\varphi_g}{\pi} \approx 1, \tag{2.13}$$

and formula (2.12) is simplified.

Integrating dS_F between the limits x_g and x'_g, we obtain S_F. We then obtain the connection between the pseudopotential and S_F, given by the following expressions:

$$\frac{S_F^0 - S_F}{S_F^0} = \sum_g \frac{1}{2}\frac{|V_g|}{E_F^0}\left[\Phi\left(\frac{p_g}{p_F^0}\right) - \frac{1}{2}\tilde{\Phi}\left(\frac{p_g}{p_F^0}, \varphi_g\right)\right], \tag{2.14}$$

$$\Phi(z) = \frac{1}{z}E(z) - \left(\frac{1}{z} - z\right)K(z), \tag{2.14a}$$

$$\tilde{\Phi}(z,\ \varphi)=\frac{1}{z}E\left(z,\ \frac{\pi}{2}-\varphi\right)-\left(\frac{1}{z}-z\right)F\left(z,\ \frac{\pi}{2}-\varphi\right)$$
$$-\frac{1}{z}\left(1-\sqrt{1-z^2\cos^2\varphi}\right)\operatorname{tg}\varphi, \qquad (2.14b)$$
$$E(z)\equiv E\left(z,\ \frac{\pi}{2}\right),\quad K(z)\equiv F\left(z,\ \frac{\pi}{2}\right), \qquad (2.14c)$$
$$E(z,\ \psi)=\int_0^{\psi}d\varphi\sqrt{1-z^2\sin^2\varphi},\quad F(z,\ \psi)=\int_0^{\psi}\frac{d\varphi}{\sqrt{1-z^2\sin^2\varphi}}; \qquad (2.14d)$$

$F(z, \psi)$ and $E(z, \psi)$ are complete elliptic integrals of the first and second kind respectively (see [54]).

The influence of the pseudopotential on $\langle v_F\rangle$ can be obtained by using the relation

$$\frac{\langle v_F\rangle}{v_F^0}=\frac{N}{N_{\text{val}}}\frac{S_F^0}{S_F}. \qquad (2.15)$$

Inasmuch as the density of the electronic states on the Fermi surface is $(dY/dE)_F \sim \oint dS_F/v_F$, it follows from (2.10a) that in the considered approximation, which is linear in $|V_g|/E_F$, we have

$$\left\langle\left(\frac{1}{v_F}\right)\right\rangle S_F=\left(\frac{1}{v_F^0}\right)S_F^0, \qquad (2.15a)$$

i.e., the periodic lattice potential does not change the density of states of the electrons on the Fermi surface. Using this circumstance and assuming that $\langle(1/v_F)\rangle \approx 1/\langle v_F\rangle$, we obtain the following relations that make it possible to estimate approximately S_F and $\langle v_F\rangle$:

$$\frac{S_F}{S_F^0}\approx\frac{\langle v_F\rangle}{v_F^0}\approx\sqrt{\frac{N}{N_{\text{val}}}}. \qquad (2.16)$$

The formulas presented above for S_F, $\langle v_F\rangle$, $\langle v_F\rangle S_F$ and $\langle(1/v_F)\rangle S_F$ are applicable to both cubic and non-cubic metals. For non-cubic symmetry, $\langle v_F\rangle S_F$ determines $\Pr\{N/m\}_{ij}$.

b) Application of the Derived Formulas to Certain Types of Structures of the Cubic System

In considering the concrete crystalline structures, it is necessary first to clarify which Fourier components are significant. Starting from the theory of weakly coupled electrons, each Fourier component of the pseudopotential can be represented in the form

$$V_{\mathcal{K}}=F_{\mathcal{K}}U_{\mathcal{K}}. \qquad (2.17)$$

Here $U_{\mathcal{K}}$ is the Fourier component of the self-consistent atomic potential, and is determined by the Fourier component of the potential of the individual ion and by the dielectric constant of the metal (the electron screening is taken into account), while $F_{\mathcal{K}}$ is a structure factor that depends only on the positions of the ions:[18,19,53]

$$F_{\mathcal{K}}=\frac{1}{N_c}\sum_{l}\exp(-i\mathcal{K}\mathbf{l}); \qquad (2.18)$$

Here N_c is the total number of unit cells per unit volume, $\mathbf{l}$ is the lattice vector corresponding to the site l. The same structure factor enters as a factor in the structure amplitude, which determines the intensity of the x-ray diffraction maxima for lattices containing only one type of atom. If the lattice is primitive, then

$$F_{\mathcal{K}}=\begin{cases}1 & \text{for } \mathcal{K}=\mathcal{K}_g,\\ 0 & \text{for } \mathcal{K}\neq\mathcal{K}_g,\end{cases}\qquad \mathcal{K}_g=2\pi\mathbf{g}. \qquad (2.19)$$

If the lattice is complex with a basis containing s atoms, then it is necessary to take into account the effects of interference of different sublattices. Let the positions of the atoms making up the basis of the complex lattice be determined by the radius vector $\mathbf{r}_n=\sum_{i=1}^{3}x_{ni}\mathbf{a}_i$ ($n = 1, 2, \ldots, s$), where $\mathbf{a}_i$ are the main lattice vectors. The Bragg plane of interest to us will be determined by the indices $(n_1n_2n_3)$. Then

$$F_{n_1n_2n_3}=\sum_{n=1}^{s}e^{2\pi i(n_1x_{n1}+n_2x_{n2}+n_3x_{n3})}. \qquad (2.20)$$

It is obvious that the only V_g that differ from zero are those for which the structure factor is not equal to zero. For optics there is an additional limitation: the only important V_g are those for which the corresponding Bragg plane intersects the sphere of the free electrons.

The radius of the free-electron sphere, as is well known, is determined by the expression

$$p_F^0=2\pi\hbar\left(\frac{3}{8\pi}\frac{\Delta n}{\Delta\tau}\right)^{1/3}; \qquad (2.21)$$

Here Δn is the number of valence electrons in the volume $\Delta\tau$.

Using (2.20) and (2.21), we can readily determine which V_g exert a strong influence on the optical properties of metals. Tables I and II list the results of calculations of F_g and p_F^0 pertaining to certain types of cubic-system structures.

By way of an example let us consider lead—a tetravalent metal with face-centered lattice. For this metal $p_F^0 = 1.24\,(2\pi\hbar/a)$ (see Table II). It follows from Table I that in this case only eight Bragg planes V_{111} and six Bragg planes V_{200} are significant. Using (2.12), we obtain

$$\frac{N_{\text{val}}-N}{N_{\text{val}}}=4{,}39\frac{|V_{111}|}{E_F^0}\left(\frac{1}{2}+\frac{\varphi_{111}}{\pi}\right)+3{,}80\frac{|V_{200}|}{E_F^0}\left(\frac{1}{2}+\frac{\varphi_{200}}{\pi}\right), \qquad (2.22)$$
$$\varphi_{111}=\operatorname{arctg}\frac{0{,}422}{|V_{111}|/E_F^0},\quad \varphi_{200}=\operatorname{arctg}\frac{0{,}313}{|V_{200}|/E_F^0}. \qquad (2.22a)$$

Relations (2.14) make it possible to calculate $(S_F^0 - S_F)/S_F^0$ in similar fashion.

Table I. Structure factors and distances to the center of the zone of different Bragg planes for certain types of structures of the cubic system

$\{n_1n_2n_3\}$	Number of planes	$P_{n_1n_2n_3}/(2\pi\hbar/a)$	$\lvert F_{n_1n_2n_3}\rvert$ face-centered	body-centered	diamond	of β-W type*	$\{n_1n_2n_3\}$	Number of planes	$P_{n_1n_2n_3}/(2\pi\hbar/a)$	$\lvert F_{n_1n_2n_3}\rvert$ face-centered	body-centered	diamond	of β-W type*
100	6	0.500	0	0	0	0	300	6	1.500	0	0	0	0
110	12	0.707	0	2	0	0 *)	310	24	1.581	0	2	0	0 *)
111	8	0.866	4	0	$4\sqrt{2}$	0	311	24	1.658	4	0	$4\sqrt{2}$	0
200	6	1.000	4	2	0	4	222	8	1.732	4	2	0	4
210	24	1.118	0	0	0	4	320	24	1.803	0	0	0	4
211	24	1.225	0	2	0	4	321	48	1.871	0	2	0	4
220	12	1.414	4	2	8	0 *)	400	6	2.000	4	2	8	8
221	24	1.500	0	0	0	0							

Here $\{n_1n_2n_3\}$ – indices of physically equivalent Bragg planes; $P_{n_1n_2n_3}$ – distance of Bragg plane to the center of the zone in momentum space; a–lattice period; $|F_{n_1n_2n_3}|$–modulus of the structure factor.

*Lattices of β-W type are known for alloys of the type $(A_3B)_2$. For these alloys, the structure factors marked by an asterisk will be different from zero, but they are still small.

Table II. Dependence of the radius of the free-electron sphere on the concentration of the valence electrons for certain types of cubic-system structures

Number of valence electrons per atoms	$p_F^0/(\frac{2\pi\hbar}{a})$				Number of valence electrons per atoms	$p_F^0/(\frac{2\pi\hbar}{a})$			
	face-centered	body-centered	diamond	of β-W type		face-centered	body-centered	diamond	of β-W type
0.5	0.620	0.492	0.782	0.782	3	1.127	0.895	1.420	1.420
0.75	0.710	0.564	0.895	0.895	4	1.241	0.985	1.563	1.563
1	0.782	0.620	0.985	0.985	5	1.337	1.061	1.684	1.684
1.25	0.842	0.668	1.061	1.061	6	1.420	1.127	1.790	1.790
1.5	0.895	0.710	1.127	1.127	7	1.495	1.187	1.884	1.884
1.75	0.942	0.748	1.187	1.187	8	1.563	1.241	1.970	1.970
2	0.985	0.782	1.241	1.241	9	1.626	1.290	2.048	2.048
2.5	1.061	0.842	1.337	1.337	10	1.684	1.337	2.122	2.122

c) Short Wave Region

We shall designate as a short wave region the spectral region in which interband transitions make an appreciable contribution to the optical constants. These are usually the visible and near-infrared regions.

An investigation of the interband transitions in metals makes it possible to determine the values of V_g. The optical method of determining the Fourier components of the pseudopotential has significant advantages over other methods, such as the van Alphen–de Haas effect or cyclotron resonance. The optical method is more direct, requires no complicated calculations, and in addition is at present the only method which makes it possible to obtain the temperature dependence of V_g. All the remaining methods are connected with measurements at low temperatures and cannot yield the temperature dependence of V_g.

It must be emphasized that the Fourier components of the pseudopotential are the main characteristics that determine not only the optical but also all other properties of metals, connected with the valence electrons and with their interaction with the lattice. The very same Fourier components with which we deal in optics determine the van Alphen–de Haas effect, the cyclotron resonance, transport phenomena, absorption of ultrasound, superconductivity, etc. Therefore the experimental determination of V_g is of great interest.

To determine V_g from optical data it is necessary to consider interband transitions connected with the corresponding Bragg planes. For the indicated transitions, there is a peak in the combined interband density of states at frequencies $\omega \approx 2|V_g|/\hbar$, leading to the appearance of maxima in the interband conductivity σ. Thus, it is possible to determine $|V_g|$ from the positions of the maxima of the function $\tilde{\sigma}(\omega)$.

Interband transitions between the electron states near the Bragg plane were considered in [20,45,46,55].* In this case it is more convenient to use the scheme of reduced bands. In Fig. 1, the band with the higher number in the scheme of the reduced bands is designated by the dashed lines. We shall need subsequently the electron wave functions normalized to a unit volume. As already indicated, for both lower and upper bands, they can be regarded as linear combinations of two plane waves:

$$\left.\begin{aligned}\psi_1 &= a_{11}\exp\left(\frac{i\,\mathbf{pr}}{\hbar}\right) + a_{12}\exp\left[\frac{i\,(\mathbf{p}-2\mathbf{p}_g)\,\mathbf{r}}{\hbar}\right],\\ \psi_2 &= a_{21}\exp\left(\frac{i\mathbf{pr}}{\hbar}\right) + a_{22}\exp\left[\frac{i\,(\mathbf{p}-2\mathbf{p}_g)\,\mathbf{r}}{\hbar}\right];\end{aligned}\right\} \tag{2.23}$$

$$\left.\begin{aligned}a_{11} &= \frac{1}{\sqrt{2}}\left(1+X^2-X\sqrt{1+X^2}\right)^{-1/2},\\ a_{12} &= a_{11}\left(X-\sqrt{1+X^2}\right),\\ a_{21} &= \frac{1}{\sqrt{2}}\left(1+X^2+X\sqrt{1+X^2}\right)^{-1/2},\\ a_{22} &= a_{21}\left(X+\sqrt{1+X^2}\right),\end{aligned}\right\} \tag{2.23a}$$

$$X = \frac{p_g}{m|V_g|}(p_g - p_\perp) = \frac{2x}{\xi}. \tag{2.24}$$

The electron energy in the upper and lower bands is determined by formula (2.6). The energy difference in transitions with conservation of the quasimomentum is

$$\Delta E = 2|V_g|\sqrt{1+X^2} = \hbar\omega_g\sqrt{1+X^2}, \tag{2.25}$$

$$\hbar\omega_g = 2|V_g|. \tag{2.26}$$

For all the points of a plane parallel to the Bragg plane we have X = const and ΔE = const. Light of frequency $\omega = \Delta E/\hbar$ can produce a transition from the lower band to the upper one for all the electrons whose state is represented by the points on the ring between the two circles obtained from the intersection of the Fermi surface with the indicated plane (ring $M_1'M_2'$ on Fig. 2). Indeed, the energy conservation law is satisfied for these electrons and, in addition, the lower state is occupied, since its energy is smaller than the Fermi energy by an amount much larger than kT, and the upper state is free, since its energy is larger than the Fermi energy by an amount much larger than kT. The minimum frequency of the interband transitions near the Bragg plane equals ω_g in this approximation. It corresponds to the ring M_1M_2 on the Bragg plane (see Fig. 2).

If we disregard relaxation processes, then in the approximation under consideration the interband conductivity $\tilde{\sigma}_g$ will have an infinitely large maximum at a frequency ω_g. Allowance for relaxation processes yields finite values for $\tilde{\sigma}_g$. The relaxation processes can be taken into account in the simplest manner by replacing the δ function, which expresses the energy conservation law, by the Lorentz function $\varphi(x) = \gamma/\pi(x^2+\gamma^2)$. The parameter γ, characterizing the smearing of the energy levels, is assumed to be constant for the transitions near the given Bragg plane. Such an allowance for the relaxation processes is possible only in the first approximation.

Let us calculate $\tilde{\sigma}_g$ —the contribution made to the interband conductivity of transitions near the Bragg plane under consideration. The value of $\tilde{\sigma}_g$ will be determined from the losses of the electromagnetic field:*

$$\tilde{\sigma}_g = \frac{W_g\hbar\omega}{\overline{\mathscr{E}^2}}; \tag{2.27}$$

here W_g is the probability of absorption per unit time of a quantum of light of frequency ω. The bar denotes averaging with respect to time. The time-dependent

*The idea of weakly coupled electrons was first used for the calculation of $\tilde{\epsilon}$ and $\tilde{\sigma}$ of alkali metals by Sergeev and Chernikhovskiĭ [56]. However, only the development of the theory of the pseudopotential has made it possible to understand the decisive role played by transitions near the Bragg plane for the determination of $\tilde{\epsilon}$ and $\tilde{\sigma}$.

*For simplicity we confine ourselves to cubic crystals.

Hamiltonian of the interaction of the electrons with the electromagnetic field $\mathscr{H}_i(t)$ is taken in the form[57]

$$\mathscr{H}_i(t) = i\frac{\hbar e}{mc}\nabla \mathbf{A}(t), \tag{2.28}$$

$$\mathbf{A}(t) = \frac{1}{2}(\mathbf{A}e^{-i\omega t} + \mathbf{A}^* e^{i\omega t}); \tag{2.29}$$

here A(t) is the vector potential of the electromagnetic field.

We neglect terms proportional to $\mathbf{A}^2$, meaning that we neglect two-photon processes compared with single-photon processes.

Taking (2.27)–(2.29) into account, we obtain the following relation:

$$\tilde{\sigma}_g = \frac{1}{8\pi^2}\frac{e^2}{m^2c^2\hbar}\frac{\omega}{\mathscr{E}^2}\int |\langle\psi_1|\nabla\mathbf{A}|\psi_2\rangle|^2 \varphi(\Delta E - \hbar\omega)\, d^3\mathbf{p}. \tag{2.30}$$

Calculation of the matrix element entails no difficulty. We note only that its magnitude is proportional to $\cos(\widehat{\mathbf{p}_g\mathscr{E}})$. Thus, light gives rise to interband transitions connected with the Bragg plane g only if the projection of the electric field of the light wave on the normal to the Bragg plane under consideration differs from zero. For cubic metals, allowance for the action of all the physically equivalent Bragg planes leads to isotropy of $\tilde{\sigma}_g$. $\tilde{\sigma}_g$ will contain only the factor $n_g/3$, where n_g is the number of physically equivalent Bragg planes. For anisotropy metals, light of different polarization will cause interband transitions connected with different Bragg planes. This circumstance can be used to identify the experimentally observed maxima of σ_g.[49,50]

Using the connection between $\mathscr{E}$ and A

$$\mathscr{E} = -\frac{1}{c}\frac{\partial \mathbf{A}}{\partial t} = +\frac{i\omega}{c}\mathbf{A}, \tag{2.31}$$

we obtain the following expression for the interband conductivity:

$$\tilde{\sigma}_g = \frac{e^2}{12\pi^2\hbar^2} p_g n_g I, \tag{2.32}$$

$$I = \frac{\gamma_g'}{\omega'}\int_0^\infty \frac{dx}{\sqrt{x^2+1}\,[(\sqrt{x^2+1}-\omega')^2+\gamma_g'^2]}; \tag{2.33}$$

Here $\omega' = \omega/\omega_g$, $\gamma_g' = \gamma_g/(\hbar\omega_g)$.

The asymptotic value of $\tilde{\sigma}_g$ when $\omega \gg \omega_g$ does not depend on γ_g and equals

$$\tilde{\sigma}_g = \frac{1}{12}\frac{e^2}{\hbar^2} p_g n_g (\omega_g/\omega)^2. \tag{2.34}$$

Calculations show[20,46] that the function $\tilde{\sigma}_g(\omega)$ has a maximum in the region $\omega_{max} \approx \omega_g$. The shift of the maximum from this position is not large. It does not exceed 6% and can be calculated by determining from experiment the relative broadening of the energy levels γ_g' This result justifies the possibility of determining the Fourier components of the pseudopotential from optical measurements.

Figures 3 and 4 show plots of $t = \omega_{max}/\omega_g$ and I_{max} against γ'. Here I_{max} is the maximum value of the integral I, considered as a function of ω'; ω_{max} is the frequency corresponding to I_{max}, i.e., $I(\omega_{max}) = I_{max}$. Using Fig. 3, we can determine $|V_g|$ more accurately from the relation

$$2|V_g| = \hbar\omega_g = \frac{\hbar\omega_{max}}{t}. \tag{2.35}$$

Figure 5 gives the form of the $I(\omega')$ curve for different values of γ'. It follows from the figure that

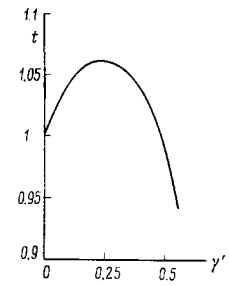

FIG. 3. Plot of $t = \omega_{max}/\omega_g$ against γ'.

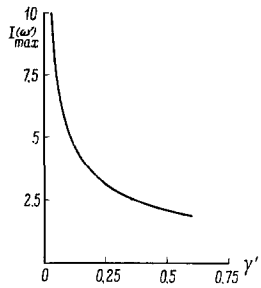

FIG. 4. Plot of the maximum value of the function $I(\omega')$ against γ'.

$$\gamma' \approx \frac{\omega_{max} - \omega_1}{\omega_{max}}, \tag{2.36}$$

where $\omega_1 < \omega_{max}$ and corresponds to the value $I \approx 0.7\, I_{max}$. Relation (2.36) is justified in greater detail in [20,46].

The considered picture of the interband transitions relates the main structure of the bands of the interband conductivity in metals with the Bragg splitting of the energy. It differs from the picture observed in semiconductors, where the main structure of the interband-conductivity bands is connected with the splitting of the energy near the critical points, which are points of high symmetry.* In metals, the points of high symmetry can also produce small maxima of interband conductivity, but these are much smaller than the maxima connected with the rings on the Bragg planes, since the number of electrons taking part in the transitions between the indicated high-symmetry points is much smaller than the

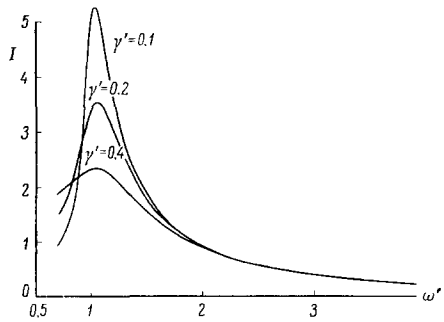

FIG. 5. Form of the $I(\omega')$ curve for three values of γ'.

*The influence of the critical points on the spectral density of lattice vibrations was considered by Van Hove [58] and by Phillips [59]. Later similar considerations were applied by Phillips [60, 61] and by Brust et al. [62] to electrons in metals. The role of critical points is also emphasized in the theoretical papers of Kohn [63] and Phillips [61].

number of electrons taking part in transitions near the rings under consideration.*

By obtaining the values of $|V_g|$ from the optical measurements in the shortwave region, we can calculate N, S_F, and $\langle v_F \rangle$. These values can be compared with the corresponding values obtained independently from measurements in the long-wave region. The indicated program is described in Ch. 6.

d) Dependence of the Main Electronic Characteristics on the Temperature

There is an established point of view, according to which the main electronic characteristics N, S_F, and $\langle v_F \rangle$ for metals do not depend on the temperature. It is based on the fact that the energy of the conduction electron $E_F \approx 10$ eV is much larger than the thermal energy kT, which at room temperature amounts to 0.02–0.03 eV.

However, the dependence of the indicated electron characteristics on T is connected not with the thermal motion of the electrons, but with the thermal motion of the ions. The lattice vibrations disturb its periodicity. This causes V_g to decrease with increasing T. As a result, N, S_F, and $\langle v_F \rangle$ increase. This question is considered in greater detail in [20,44].

The $V_g(T)$ dependence is connected with the fact that, according to (2.17), the Fourier component of the pseudopotential is proportional to the structure factor defined by formula (2.18). The thermal vibrations of the lattice cause the structure factor to contain a temperature factor $\exp[-W(T)]$, called the Debye-Waller factor. A similar factor determines the intensity of the diffraction maxima in the "x-ray band".[64,65]

The procedure for obtaining this factor is standard.[19] The radius vector of the site l is represented in the form

$$\mathbf{R}_l = \mathbf{l} + \mathbf{u}_l = \mathbf{l} + \sum_q \frac{1}{\sqrt{2}} [\mathbf{u}_q \exp(i\mathbf{ql}) + \mathbf{u}_q^* \exp(-i\mathbf{ql})]; \qquad (2.37)$$

Here $\mathbf{u}_q$ is the vector amplitude of the lattice vibrations, including the time factor $\exp(-i\Omega_q t)$, and $\mathbf{q}$ is the wave vector of the lattice vibrations. Subsequently, $\mathbf{R}_l$ is substituted in (2.18) in lieu of $\mathbf{l}$. Recognizing that the $\mathbf{u}_q$ are small, we expand the corresponding exponentials in series. The obtained expressions contain terms that have factors in the form $\exp(\pm i\mathbf{q}\cdot\mathbf{l})$ corresponding to creation or annihilation of phonons, as well as terms without the indicated factors, corresponding to phononless processes. Gathering the phononless terms back into an exponential, we obtain the temperature factor $\exp(-W_{\mathscr{K}})$, where

$$W_{\mathscr{K}} = \frac{1}{2} \sum_q |\mathscr{K}\mathbf{u}_q|^2. \qquad (2.38)$$

Hence

$$F(\mathscr{K}) = e^{-W_g(T)} F_g \delta(\mathscr{K} - \mathscr{K}_g) \qquad (2.39)$$

and the temperature factor enters in V_g. With our degree of accuracy, we can insert the obtained functions $V_g(T)$ into formulas (2.12), (2.14), and (2.15), and determine the temperature dependences of the quantities N, S_F, and $\langle v_F \rangle$.

To estimate the effect we must find $W_g(T)$. An exact calculation of this quantity calls for summing over the entire spectrum of the elastic oscillations. This calculation is very cumbersome. However, we can estimate the order of magnitude of W_g and the character of its temperature variation by using the Debye model of a solid. In this model, the solid is regarded as a continuous medium, i.e., the Brillouin zone is replaced by the Debye sphere. We assume for simplicity that the velocities of all three branches of the acoustic spectrum are the same. In such a model, all three modes are degenerate for each value of $\mathbf{q}$. We choose the polarization vectors such that one oscillation has $\mathbf{u}_q \parallel \mathscr{K}$, and two others have $\mathbf{u}_q \perp \mathscr{K}$. Then $W = \frac{1}{2}\mathscr{K}^2 \sum_q |\mathbf{u}_q|^2$. The obtained relation is best satisfied for cubic crystals consisting of atoms of only one type. Bearing principally this case in mind, and taking into account the connection between the oscillation amplitude and the average oscillation energy (see, for example, [19]), we obtain

$$W(T) = \frac{3}{2}\mathscr{K}^2 \frac{\hbar^2}{Mk\Theta} \left(\frac{T}{\Theta}\right)^2 \int_0^{\Theta/T} \left(\frac{1}{\exp z - 1} + \frac{1}{2}\right) z\,dz; \qquad (2.40)$$

Here M is the atom mass and Θ is the Debye temperature.

The function

$$\varphi(x) = \frac{1}{x} \int_0^x \frac{z\,dz}{\exp z - 1} + \frac{x}{4},$$

differs from the known Debye function by an amount x/4. The values of the Debye function are tabulated in [64,66]. Thus, recognizing that $\mathscr{K}\hbar = 2p_g$, we obtain

$$W_g(T) = \frac{1}{x} W_g(0) \cdot 4\varphi(x), \quad x = \Theta/T, \qquad W_g(0) = \frac{3}{2}\frac{p_g^2}{M}\frac{1}{k\Theta}. \qquad (2.40a)$$

The dependence of the ratio W(T)/W(0) on T/Θ has been calculated in [20,44].

As indicated above, the Debye-Waller factor determines also the temperature variation of the intensity of the diffraction maxima. For x-radiation, the temperature factor of the intensity is equal to $\exp(-2W)$, and p_g should be replaced by $2\pi\hbar \sin\theta/\lambda$ (θ—diffraction angle, λ—length of the x-ray wave). Thus, we can use x-ray measurements to calculate the temperature variation of N and compare it with the results of optical experiments. Since the x-ray measurements are usually performed in the range from room temperatures to nitrogen temperatures, let us calculate the change of N in this interval. The different terms under the summation sign in (2.12) have different temperature factors, since they have different p_g. To estimate the value of interest to us, we introduce a certain mean value $\overline{W}(T)$. In the temperature interval indicated above, W is small and $\exp(-W) \approx 1 - W$. Under these assumptions we obtain

$$\frac{N(T_r)}{N(T_N)} - 1 \approx \left[\frac{N_{\text{val}}}{N(T_N)} - 1\right] [\overline{W}(T_r) - \overline{W}(T_N)]; \qquad (2.41)$$

here T_r and T_N are the room temperature and nitrogen temperature, respectively.

The results obtained in this section will be compared with the experimental data in Ch. 6.

*We note in addition that the points located on the ring M_1M_2 (see Fig. 2) are not high-symmetry points and that in the transitions under consideration, both the lower and the upper states have an energy that differs from the Fermi energy by an amount much larger than kT.

3. METHODS OF MEASURING THE OPTICAL CONSTANTS OF METALS AND METHODS OF PREPARING THE SAMPLES

a) Methods of measuring n and κ

A review of methods of measuring the optical constants of metals, employed up to 1955 and intended principally for measurements in the visible and in the near-ultraviolet regions is contained in [1]. New recently developed methods can be successfully applied also to the infrared band. In this chapter we shall discuss the most promising of these methods, namely polarization methods and methods based on the measurement of the coefficient of reflection of light under normal incidence, with subsequent application of dispersion relations of the Kramers-Kronig type. In both cases one investigates the reflected light. Only the reflected light can yield the constants pertaining to a bulky undistorted metal. Indeed, an investigation of transmitted light calls for the use of very thin layers, the properties of which differ from the properties of bulk metal. The indicated methods can be used in a wide spectral interval, including the ultraviolet, the visible, and the infrared regions. The accuracy and reliability of the polarization methods is higher.

Polarization methods are connected with the measurement of the ellipticity of the light. Linearly polarized light incident on the boundary of a metal at an angle $\varphi \neq 0$ is elliptically polarized after reflection from the metal. By measuring the phase shift Δ between the p- and s-components of the reflected light and the azimuth ρ ($\tan\rho$ determines the ratio of the amplitudes of the reflected light), we obtain two relations from which n and κ are determined.

If the inequality $1/|\epsilon'| \ll 1$ is satisfied, then

$$n = \frac{\sin\varphi\cdot\operatorname{tg}\varphi\cdot\cos 2\rho}{1-\sin 2\rho\cdot\cos\Delta}, \tag{3.1}$$

$$\varkappa = \frac{\sin\varphi\cdot\operatorname{tg}\varphi\cdot\sin 2\rho\cdot\sin\Delta}{1-\sin 2\rho\cdot\cos\Delta}. \tag{3.2}$$

The minus sign in the denominator takes into account the fact that in the case of normal incidence the p- and s-components of the reflected light have a phase shift $\Delta = 0$.

In the infrared region, the indicated inequality is always satisfied for metals, and formulas (3.1) and (3.2) can be used. In the visible region of the spectrum, the value of $|\epsilon'|^{-1}$ may become appreciable. This means that it is necessary to take into account the dependence of the surface impedance on the angle of incidence. Allowance for first-order terms in $|\epsilon'|^{-1}$ gives the following connection between the complex refractive index, which we denote in this case by $\tilde{n} - i\tilde{\kappa}$, on the one hand, and Δ and ρ on the other:

$$\tilde{n} = n\left(1+\frac{1}{2}\frac{\sin^2\varphi}{n^2+\varkappa^2}\right), \tag{3.3}$$

$$\tilde{\varkappa} = \varkappa\left(1-\frac{1}{2}\frac{\sin^2\varphi}{n^2+\varkappa^2}\right); \tag{3.4}$$

Here n and κ are given by formulas (3.1) and (3.2). We shall henceforth denote the optical constants by n and κ without the superior tilde sign.

The obtained values of the optical constants make it possible to determine the absorbtivity and reflectivity A and R of the metal for normal incidence of light. As is well known,

$$A = \frac{4n}{(n+1)^2+\varkappa^2}, \quad R = \frac{(n-1)^2+\varkappa^2}{(n+1)^2+\varkappa^2}, \quad R+A=1. \tag{3.5}$$

Measurement of Δ and ρ in the visible and ultraviolet spectral regions can be readily carried out with the aid of compensators and polarizers (see the review [1]). There are no compensators for the infrared region, therefore Δ must be determined by other methods. In [20,32,36,47-48,67-69,70-71], they determined the phase shift $\Delta = \pi(2k-1)/2$ or $\Delta = \pi k$; here k is an integer. It turns out here that the use of multiple reflection of light makes it possible to increase greatly the accuracy of the measurement. This is clearly seen from the following relation:

$$\frac{r_p^{(m)}}{r_s^{(m)}} = \frac{A_p}{A_s}(\operatorname{tg}\rho)^m e^{im\Delta}; \tag{3.6}$$

Here $r_p^{(m)}$ and $r_s^{(m)}$ are the components of the electric vector of the reflected light wave after m-fold reflection from a metallic mirror, A_p and A_s are the components of the incident light wave, Δ is the phase shift after single reflection, and ρ is the azimuth after single reflection.

Thus, the phase shift increases by a factor m, i.e., $\Delta_m = m\Delta$, and the resultant azimuth is determined from the relation $\tan\rho_m = (\tan\rho)^m$. The use of multiple reflection makes is possible to operate with smaller light-incidence angles thereby facilitating the investigation of longer wavelengths.

To increase the measurement accuracy, a modulation null method is used. A block diagram of the method is shown in Fig. 6. The illuminator produces a parallel

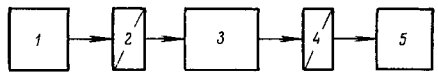

FIG. 6. Block diagram of the polarization method. 1—Illuminator, 2—polarizer, 3—investigated mirrors, 4—analyzer, 5—radiation receiver.

beam of unpolarized light. This light, passing through the polarizer, becomes linearly polarized and is incident on a system of investigated mirrors, where it experiences multiple reflection. The elliptically polarized light obtained as a result of these reflections passes through a second polarizer, which we call an analyzer, and is incident on the radiation receiver. For the modulation of the light, one uses either the rotation of one of the polarizers, or a special shutter, not shown in Fig. 6. The former method is used when the phase shift $\Delta = \pi(2k-1)/2$ is measured, and the latter when $\Delta = \pi k$ is measured. The measurements are carried out in monochromatic light from a monochromator which is placed either in a block called the illuminator or in a block called the light receiver. The position of the monochromator is not immaterial. It must be placed in that block which is connected with the immobile polarizer or analyzer, so that the polarization of the light caused by the monochromator does not come into play.

The intensity of the light passing through the polarizer-sample-analyzer system is

$$I = \frac{1}{2}I_0\left\{\left(\frac{r_p}{A_p}\right)^{2m}\cos^2\alpha_p\cdot\cos^2\alpha_A + \left(\frac{r_s}{A_s}\right)^{2m}\sin^2\alpha_p\cdot\sin^2\alpha_A\right.$$

$$+\frac{1}{2}\left(\frac{r_p}{A_p}\right)^m\left(\frac{r_s}{A_s}\right)^m \sin 2\alpha_p \cdot \sin 2\alpha_A \cdot \cos\Delta_m\Big\}; \qquad (3.7)$$

Here α_p and α_s are the azimuths of the polarizer and the analyzer. We see that α_p and α_s enter in expression (3.7) in exactly the same manner.

Let us consider a variant with a rotating polarizer. For the resultant intensity it is immaterial whether we rotate the polarizer or the analyzer. For concreteness, we assume that we rotate the polarizer with a frequency Ω, i.e., $\alpha_p = \Omega t$, where t is the time; then

$$I = A + B\cos(2\Omega t + \gamma). \qquad (3.8)$$

The quantities A, B, and γ do not depend on the time. It is seen from (3.7) and (3.8) that the alternating signal vanishes when the following conditions are satisfied:

$$\cos\Delta_m = 0, \qquad \operatorname{tg}^2\alpha_A = \left(\frac{r_p}{r_s}\right)^{2m}. \qquad (3.9)$$

Let us consider a variant with an additional rotating shutter, which must be placed ahead of the polarizer so as to eliminate the signal connected with the radiation from the investigated mirrors themselves. The angle α_A (or α_p) is set equal to 45°. It then follows from (3.7) that the signal vanishes under the following conditions:

$$\cos\Delta_m = -1, \qquad \operatorname{tg}\alpha_p = \left(\frac{r_p}{r_s}\right)^m, \qquad (3.10a)$$

or

$$\cos\Delta_m = +1, \qquad \operatorname{tg}\alpha_p = -\left(\frac{r_p}{r_s}\right)^m. \qquad (3.10b)$$

Considering the conditions (3.9) and (3.10), we see that the use of a rotating polarizer has two advantages over the use of an additional shutter. First, in the former case the minimum phase shift, which equals 90°, occurs at smaller angles of incidence of the light on the investigated mirrors than in the latter case, where it equals 180°. This makes it possible to investigate longer wavelengths with a smaller number of reflections. Second, less stringent requirements are imposed in the former case on the quality of the polarizers than in the latter case. Indeed, conditions (3.9) and (3.10) are equivalent to obtaining circular and linear polarization, respectively. In detection of the signal by means of a rotating polarizer, we obtain a zero signal already in the presence of a small part of unpolarized light transmitted by the polarizer, whereas in the case when a linearly-polarized light is obtained, this small part of the unpolarized light does not make it possible to obtain an absolute null of the signal (a more or less deep minimum is obtained).

In the investigation of both variants, we can operate in two ways: 1) the wavelength of the light λ is set and the light-incidence angle φ and the azimuth of one of the polarizers are varied until the signal vanishes. This yields values of φ and four values of α, making it possible to determine $2\rho_m$ corresponding to the given value of Δ_m. 2) The angle of incidence φ is set, and the wavelength of the light λ and the azimuth of one of the polarizers are varied until the signal vanishes. The four corresponding values of α make it possible to determine analogously ρ_m. A more detailed description of the indicated methods, and also of the experimental setups used to realize these methods, are found in the papers cited at the beginning of this chapter.

One more modification of the polarization method is based on measurement of the intensity of the reflected light under certain specially chosen polarizer positions. If, according to [72], one measures the following intensities: $I(\pi/4, 0)$, $I(\pi/4, \pi/2)$, and $I(\pi/4, \pi/4)$ then, as follows from (3.7), we get

$$(\operatorname{tg}\rho)^m = \sqrt{\frac{I\left(\frac{\pi}{4}, 0\right)}{I\left(\frac{\pi}{4}, \frac{\pi}{2}\right)}}, \qquad (3.11a)$$

$$\cos\Delta_m = \left[\frac{2I\left(\frac{\pi}{4}, \frac{\pi}{4}\right)}{I\left(\frac{\pi}{4}, \frac{\pi}{2}\right)} - 1 - (\operatorname{tg}\rho)^{2m}\right]\cdot\frac{1}{2(\operatorname{tg}\rho)^m}; \qquad (3.11b)$$

The arguments of I are in this case the azimuths of the polarizer and of the analyzer. It is possible to use also other polarizer orientations. Thus, in [73], the accuracy of the method was increased by using the relation

$$(\operatorname{tg}\rho)^m = \sqrt{\frac{I(0,0)}{I\left(\frac{\pi}{2}, \frac{\pi}{2}\right)}}\left(\frac{A_p}{A_s}\right)^m. \qquad (3.11c)$$

This method results in a somewhat lower accuracy in the determination of the optical constants, since it is not a null method and is more sensitive than the polarization methods described above to the quality of the polarizers and to the accuracy with which the optical systems are adjusted.

The second group of methods, which is also widely used, calls for the measurement of only the reflection coefficient for normal incidence of light. These measurements should be performed in a sufficiently broad spectral interval. The indicated method was developed by a number of authors.[74-78] It is described in detail in the review by Stern.[79]

The gist of the method reduces briefly to the following. One measures in the experiment the reflection coefficient for normal incidence $|r(\omega)|^2$ in a wide spectral interval $\omega_1 \le \omega \le \omega_2$. From Fresnel's formulas for the normal incidence of light we have

$$r = \frac{n - i\varkappa - 1}{n - i\varkappa + 1} = |r|\exp(i\theta). \qquad (3.12a)$$

We consider further the complex function

$$\ln r = \ln|r| + i\theta. \qquad (3.12b)$$

We obtain for it dispersion relations of the Kramers-Kronig type, relating the real and imaginary parts of the complex dielectric constant.[80] As a result we get the following equation for the phase θ:

$$\left.\begin{aligned} \theta(\omega) &= \frac{2\omega}{\pi}\int_0^\infty \frac{\ln|r(\omega')|}{\omega'^2 - \omega^2}\,d\omega', \\ \text{or} \quad \theta(\omega) &= \frac{1}{\pi}\int_0^\infty \frac{d\ln|r(\omega')|}{d\omega'}\ln\left|\frac{\omega'+\omega}{\omega'-\omega}\right|d\omega'. \end{aligned}\right\} \qquad (3.13)$$

Since the measurements are usually carried out in a limited interval $\omega_1 \le \omega \le \omega_2$, the value of $|r(\omega)|$ is extrapolated both towards longer wavelengths $\omega < \omega_1$ and towards shorter wavelengths $\omega > \omega_2$. The extrapolation law is chosen such as to have n and κ coincide with the directly measured values of these constants in some region of the spectrum.

This method was used by various authors to determine the optical constants of a number of metals and semiconductors at room temperature (see, for example, [77,78,81-87]).

A weak aspect of the last method is the need for extrapolation of $|r(\omega)|$, and since the extrapolation is not unique, the accuracy and reliability of the results are reduced.

We shall not analyze here other methods of measuring the optical constants of metals (for example interference methods), since they are much less promising for measurements in a broad spectral range. All are discussed in a number of review papers (see, for example [1,35,88-89]).

Modern methods make it possible to determine the optical constants of good metals with an accuracy 1–2%.

b) Methods of Sample Preparation

We are interested in the optical constants of bulk metals. Therefore the methods of preparing the samples for the investigation should result in samples that satisfy a number of requirements. First, since the light penetrates into the metal to a depth of the skin layer, $\sim 2 \times 10^{-6}$ cm, it is necessary that the properties of this layer coincide or be very close to the properties of the bulk metal. Second, the surface of the metal should be plane and mirror-finished. Third, the total thickness of the layer of metal should be sufficiently large so as not to take into account reflection from the other surface (this requirement is not essential).

At the present time there are two methods that yield samples satisfying the foregoing requirements,* evaporation of the metal in vacuum and its condensation on polished substrates, or electric polishing.

The method of evaporation of metals in vacuum requires a separate choice, for each metal, of the evaporator material, the evaporation conditions, and the method of preparing the substrate. In the investigations reported in [20,31-32,36,40,47-48,90-92], the quality of the obtained layers was monitored continuously both when determining the evaporation conditions and when preparing the samples for the investigation. Particular attention was paid to the density, conductivity, temperature dependence of the conductivity, and the residual resistivity of the metallic layers. Certain other characteristics of these layers were also determined. As a result, it was possible to obtain good mirror-finish layers with properties that coincide with or are very close to the properties of the bulky metal. The cited papers describe the evaporation conditions of the investigated metals and the preparation of the substrates for the sputtering.

The method of electric polishing also calls for special control. Before the electric polishing, the samples are ground and polished mechanically, and this results in a case-hardened layer. The electric-polishing conditions should be chosen such as to remove the entire case-hardened layer and at the same time leave the metal surface sufficiently flat and brilliant. A good way of monitoring the complete removal of the case-hardened layer is to use x-ray and electron-diffraction investigations of the metal surface. The case-hardened layer, in the case of polycrystalline samples, produces broad smeared diffraction rings, which become narrower as the layer is removed. Starting with a certain thickness of the removed layer, the rings stop narrowing, and this can indicate that the case-hardened layer has been completely removed.* By way of an example we indicate that for tungsten and its alloys, it is sufficient to remove by electric polishing a layer of $\sim 15\ \mu$, for neobium and its alloys with titanium it is necessary to remove a layer $\sim 50\ \mu$ thick,[93-94] and for aluminum it is necessary to remove a layer $\sim 100\ \mu$ thick. Thus, by carrying out suitable control measurements, it is possible to obtain by the indicated methods samples of the required quality.

Let us stop to discuss the influence of oxidation of the metal surface. The experiments have shown that by evaporation in vacuum it is possible to make the specular surfaces of many metals, such as indium, lead, tin, gold, [20,32] so good that their oxidation proceeds very slowly. Measurements of n and κ, performed both immediately after the preparation of the samples and after leaving the samples for a day in the apparatus, have shown that no changes take place in n or κ. Even in such a lightly oxidizing metal as lead, noticeable changes occur only after several days. In [95-97], the rate of oxidation of the investigated layers was larger. But even for these layers, control measurements performed by the authors of the cited papers have shown that the thickness of the oxide layer is small.† Since the effects which we shall consider are of the order of unity, a slight influence of the oxide layer, on the order of 10%, can be neglected.

4. OPTICAL CONSTANTS OF NON-TRANSITION METALS

In a brief review it is impossible to present the results of the measurements of the optical constants of all the non-transition metals. We shall pay particular attention to polyvalent metals. The influence of the lattice on the behavior of the valence electrons of these metals is stronger than in the case of monovalent metals.‡

To obtain maximum information concerning the electron structure of metals from optical investigations, the latter should satisfy a number of requirements. First, it is necessary to measure both the optical constants n and κ (or the real and imaginary parts of the complex dielectric constant). Second, the spectral interval of the investigation should be sufficiently broad. To obtain characteristics pertaining to the conduction electrons as well as to the electrons that take part in the interband transitions, this interval must include both the infrared and the visible regions of the spectrum. Third, the measurements should be carried out in a wide temperature interval. Particular interest attaches to measurements at helium temperatures, since the determination of the Fourier components of the pseudopotential by an optical method is carried out most accurately at

*Special notice should be taken of the fact that mechanical polishing does not produce samples of the required quality, owing to the case-hardened layer.

*For single crystals, a similar criterion is afforded by the width of the diffraction spots.

†Formulas for taking into account the influence of surface oxide layers on the results of metal-optical measurements are given in [98].

‡A discussion of the optical properties of noble monovalent metals is contained in the review of Suffczynski [99] and in the papers of Ehrenreich, Cooper, Phillipp [82–84] and Beaglehole [100]. The optical properties of alkali metals are considered in a paper by Mayer and Hietel [101].

these temperatures. The use of a wide temperature interval for the optical investigations makes it possible to obtain the temperature dependence of the main electronic characteristics. Fourth, comprehensive measurements are needed, i.e., the main optical measurements should be supplemented by measurements of many other properties of the samples (structure, density, static conductivity, etc.). Only such comprehensive investigations will make it possible to obtain samples of the required quality and to determine more fully the microscopic characteristics of the metals.

At the present time, investigations satisfying the foregoing requirements were performed only for indium[47] and lead.[48] The results of the measurements of n and κ for these metals are presented below in the form of tables.* We present also the most reliable results for tin,[36,69,102] aluminum,[90,96-97] and zinc.[49,103] Investigations of these metals were made in less detail and call for further measurements from the point of view indicated above. For many other polyvalent nontransition metals, such as gallium, thalium, beryllium, magnesium, and cadmium, we confine ourselves only to references to the available literature, for in the case of these metals it is necessary above all to verify the quality of the investigated samples.

It should be noted that the lack of data on the sample quality does not make it possible to use the results of most of the earlier investigations. The point is that different sample-preparation methods can yield different structures of the investigated layer, and this can lead to appreciable changes in the properties determined by the valence electrons, particularly the conduction electrons, and their interaction with the lattice (owing to the change in the band structure and the additional scattering, which is connected with impurities, crystal-lattice defects, and crystallite boundaries).

The results obtained by a number of authors, besides lacking data on the quality of the investigated samples, are not useable also because they are presented not in the form of tables, but in the form of plots with very inconvenient scales. It is impossible to determine n and κ from these plots with any degree of accuracy. The foregoing pertains, in particular, to the work of Hodgson,[104,105] Woodall, Lenham, and Treherne,[106-108] and a few others.

Before we present tables of experimental values for a number of polyvalent metals, let us consider the qualitative picture of the dependence of n and κ on λ and T. Figures 7–10 show by way of an example the results of the measurements of the optical constants of lead.

As follows from Figs. 7 and 9, the experimental functions $n(\lambda)$ and $\kappa(\lambda)$ are monotonically increasing in the long-wave region. The temperature measurements in this region have shown that the n(T) dependence is significant over the entire interval. When the temperature is lowered, as expected, n decreases. This decrease is significant not only on going from room temperature to nitrogen temperature, but also on going from nitrogen temperature to helium temperature. The κ(T) dependence for this interval is more appreciable in the long-wave end of the interval, where κ increases strongly with decreasing temperature. On going from room temperature to nitrogen temperature, κ changes much more

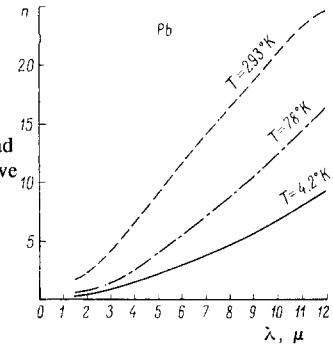

FIG. 7. Dependence of n of lead on λ at three temperatures (long-wave region).

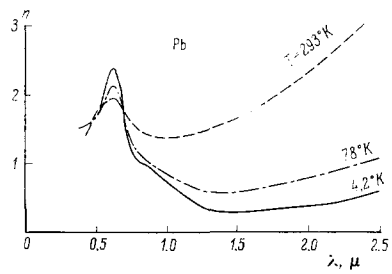

FIG. 8. Dependence of n of lead on λ at three temperatures (short-wave region).

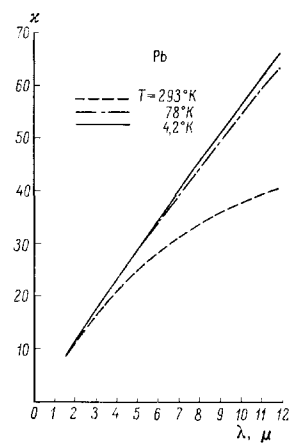

FIG. 9. Dependence of κ of lead on λ at three temperatures (long-wave region).

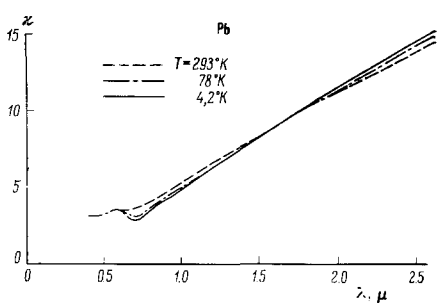

FIG. 10. Dependence of κ of lead on λ at three temperatures (short-wave region).

*The results of the measurements of the optical and many other properties of the investigated samples of indium, lead, aluminum, and tin are described in greater detail in [20].

than on going from nitrogen temperature to helium temperature. On the whole, the dependence of κ on the temperature is much weaker than the dependence of n on the temperature.

It follows from Figs. 8 and 10 that the function $n(\lambda)$ has maxima in the short-wave region. The magnitude and widths of the maxima depend on the temperature. With decreasing temperature, the maxima become narrower and larger. The function $\kappa(\lambda)$ has singularities in the same spectral regions as $n(\lambda)$, but they are much less pronounced.

We present tables III–VII of the experimental data of n and κ of certain non-transition metals of groups 4, 3, and 2.

Each table contains also references to papers not used in the present review, since they did not satisfy the conditions indicated above (see also Table VIII). The results pertain to polycrystalline samples. We shall not

Table III. Optical constants of lead* (from [48])

λ, μ	T = 293° K		T = 78° K		T = 4,2° K		λ, μ	T = 293° K		T = 78° K		T = 4,2° K	
	n	κ	n	κ	n	κ		n	κ	n	κ	n	κ
0.45	1.44_5	3.18	1.56	3.20	—	—	0.95	1.38_5	4.99	0.917	4.67	0.821	4.57
0.46	1.54_5	3.20	1.57_5	3.22	—	—	1.00	1.38	5.32	0.848	5.00	0.721	4.90
0.48	1.62	3.25	1.65	3.22	—	—	1.05	1.38_5	5.62	0.801	5.30	0.656	5.22
0.50	1.70_5	3.30	1.67_5	3.24	—	—	1.10	1.40	5.98	0.743	5.63	0.574	5.58
0.52	1.75_5	3.34	1.70	3.31	—	—	1.15	1.41_5	6.31	0.678	6.00	0.485	5.92
0.54	1.81	3.37	1.78	3.39	1.82	3.46	1.20	1.44_5	6.59	0.651	6.28	0.417	6.29
0.56	1.87	3.41	1.87_5	3.45	1.97	3.51	1.30	1.50	7.23	0.583	6.96	0.312	6.96
0.58	1.90	3.43	1.96_5	3.47	2.11	3.52	1.40	1.58	7.74	0.566	7.59	0.285	7.59
0.59	1.91	3.44	2.01	3.46	2.17	3.52	1.50	1.64_5	8.30	0.575	8.23	0.275	8.24
0.60	1.91_5	3.45	2.06	3.44	2.26	3.50	1.60	1.77_5	8.90	0.611	8.93	0.300	8.94
0.61	1.94_5	3.46	2.10	3.42	2.29	3.45	1.80	2.05	10.1_5	0.683	10.2	0.336	10.3_5
0.62	1.94_5	3.47	2.11	3.38	2.34	3.38	2.00	2.32	11.2	0.783	11.3_5	0.387	11.5_5
0.64	1.94_5	3.49	2.13	3.28	2.39	3.16	2.20	2.63	12.2	0.901	12.5_5	0.448	12.7_5
0.66	1.89_5	3.51	2.08	3.19	2.28	3.02	2.40	3.03	13.2	0.997	13.7_5	0.541	13.9_5
0.68	1.85_5	3.53	1.96_5	3.10	2.09	2.89	2.60	3.45	14.4_5	1.19_5	14.8_5	0.614	15.0_5
0.70	1.78_5	3.57	1.80	3.07	1.85	2.82	3.0	4.27	16.4	1.53	17.3	0.81	17.3
0.72	1.71	3.64	1.58	3.13	1.54_5	2.89	3.5	5.39	18.6	2.01	20.4	1.10	20.1
0.74	1.63_5	3.73	1.39	3.24	1.30_5	3.06	4.0	6.58	20.8	2.48	22.9	1.49	23.1
0.76	1.57	3.84	1.28	3.41	1.17_5	3.26	5.0	9.04	24.8	3.99	28.7	2.15	28.6
0.78	1.52_5	3.96	1.18_5	3.58	1.09	3.46	6.0	11.7	28.1	5.41	33.9	2.95	34.4
0.80	1.50_5	4.09	1.13	3.73	1.04	3.61	7.0	14.1	30.9	7.16	38.7	3.75	39.9
0.82	1.47	4.18	1.09	3.86	1.00_5	3.78	8.0	16.4	33.6	8.82	43.9	4.50	45.5
0.85	1.44	4.35	1.05_5	4.05	0.976	3.97	9.0	18.7	35.8	10.5	49.1	5.56	50.6
0.88	1.41	4.56	1.01	4.25	0.940	4.16	10.0	21.0	37.4	12.3	54.4	6.70	55.9
0.90	1.40	4.68	0.983	4.37	0.904	4.27	11.0	23.2	39.2	14.4	59.1	7.90	61.3
							12.0	24.6	40.5	16.3	63.5	9.20	66.5

The optical constants of lead were investigated also in [30–32, 67, 113]

*In this review we publish only part of the experimental data of [48]. A more complete table can be found in the cited paper.

Table IV. Optical constants of tin

λ, μ	T = 293° K		T = 78° K		T = 4,2° K		λ, μ	T = 293° K		T = 78° K		T = 4,2° K	
	n	κ	n	κ	n	κ		n	κ	n	κ	n	κ
a) Infrared region (from [36, 69]).													
0.73	2.18	6.29	2.24	6.19	—	—	3.0	4.41	17.8	1.88	18.0	1.58	18.0
0.80	2.40	6.62	2.27	6.42	—	—	3.5	5.27	20.5	2.13	21.1	1.95	21.1
0.93	3.15	7.28	3.43	7.17	2.95	7.62	4.0	6.19	23.2	2.46	24.2	2.13	24.2
0.99	3.44	7.34	3.92	6.94	3.70	7.15	5.0	8.49	28.5	3.75	29.7	2.75	30.0
1.20	3.76	7.63	3.53	6.45	3.05	5.98	6.0	11.0	33.1	4.97	35.5	3.73	35.8
1.35	3.57	8.04	2.76	6.99	2.55	6.64	7.0	13.8	37.1	6.51	41.4	4.89	41.6
1.50	3.31	8.67	2.09	7.98	1.99	7.80	8.0	16.6	40.6	8.17	47.0	6.05	47.4
1.70	3.13	9.88	1.75	9.29	1.51	9.35	9.0	19.3	43.8	10.0	51.7	7.90	53.3
2.00	3.10	11.8	1.65	11.4	1.38	11.4	10.0	22.0	46.4	12.4	55.8	10.1	58.7
2.50	3.63	14.8	1.69	14.6	1.39	14.6	11.0	24.8	49.0	15.7	59.8	12.6	63.4
							12.0	27.8	51.6	18.2	63.8	15.3	67.0

λ, μ	n	κ	λ	n	κ	λ	n	κ
b) Visible and ultraviolet regions (at T = 293°K, from [102]).								
0.668	1.418	5.007	0.468	0.703	3.124	0.347	1.012	2.227
0.620	1.249	4.789	0.447	0.722	2.911	0.325	0.980	2.396
0.588	1.121	4.512	0.425	0.701	2.487	0.298	1.037	2.762
0.533	0.889	3.922	0.398	0.676	1.906	0.275	1.119	3.308
0.502	0.780	3.575	0.361	0.905	1.931	0.257	1.117	3,333
0.480	0,709	3.318						

In the region 0.6 – 0.7μ, the data of the cited papers are subject to a slight discrepancy, which is probably connected with the inaccuracy of the measurements of the optical constants for the extreme points of the employed spectral interval.

The optical constants of tin were investigated also in [67, 104, 106, 110 – 112, 113 – 115].

Table V. Optical constants of indium (from [47])

λ, μ	T = 295° K		T = 4,2° K		λ, μ	T = 295° K		T = 4,2° K	
	n	ϰ	n	ϰ		n	ϰ	n	ϰ
0.55	0.70	4.70	0.695	4.70	1.85	—	—	1.70	13.5
0.60	0.795	5.02	0.77	5.08	1.90	2.80	13.8	1.75	13.85
0.65	0.90	5.42	0.835	5.50	1.93	—	—	1.78	14.2
0.70	1.01	5.83	0.99	6.00	2.00	2.97	14.5	1.84	14.6
0.72	1.07	6.00	1.09	6.20	2.05	—	—	1.88	14.8
0.74	1.13	6.18	1.20	6.40	2.10	3.13	15.0	1.92	15.0
0.75	1.17	6.26	1.26	6.45	2.15	—	—	1.96	15.3
0.76	1.19	6.31	1.33	6.50	2.20	3.30	15.6	1.98	15.6
0.80	1.32	6.60	1.59	6.65	2.25	—	—	1.99	16.0
0.82	—	—	1.65	6.68	2.30	3.48	16.3	2.00	16.2
0.85	1.45	6.78	1.71	6.72	2.35	—	—	2.00	16.5
0.90	1.59	7.18	1.73	6.85	2.40	3.65	16.9	1.99	16.8
0.95	1.72	7.44	1.65	7.00	2.45	—	—	1.97	17.2
1.00	1.81	7.77	1.49	7.25	2.50	3.81	17.6	1.95	17.5
1.05	—	—	1.41	7.60	2.55	—	—	1.93	17.8
1.10	1.84	8.38	1.35	8.00	2.60	4.00	18.3	1.92	18.25
1.15	—	—	1.31	8.42	3.0	4.70	20.9	1.90	20.9
1.20	1.87	9.00	1.28	8.88	3.5	6.0	23.9	2.05	23.9
1.25	—	—	1.28	9.24	4.0	7.27	26.7	2.3	26.7
1.30	1.95	9.70	1.30	9.60	5.0	9.77	32.2	3.1	32.7
1.35	—	—	1.32	9.95	6.0	12.4	37.2	4.2	38.7
1.40	2.06	10.35	1.35	10.3	8.0	18.4	45.3	7.5	50.6
1.45	—	—	1.36	10.6	10.0	24.8	51.9	13.5	62.3
1.50	2.19	11.0	1.39	10.9					
1.55	—	—	1.45	11.45					
1.60	2.33	11.8	1.48	11.9					
1.65	—	—	1.52	12.2					
1.70	2.49	12.5	1.56	12.6					
1.75	—	—	1.61	12.9					
1.80	2.64	13.1	1.65	13.2					

The optical constants of indium were investigated also in [40, 95–97, 106–107, 110, 116–118].

Table VI. Optical constants of aluminum

λ, μ	T = 295° K		T = 78° K		λ, μ	T = 295° K		T = 78° K	
	n	ϰ	n	ϰ		n	ϰ	n	ϰ
a) Infrared region (from [90]).									
1.20	0.95	9.6	0.63	9.6	5.0	6.7	37.6	4.4	37.8
1.50	1.14	12.1	0.78	12.1	6.0	9.5	44.4	6.5	44.9
2.00	1.75	16.1	1.30	16.1	7.0	12.6	51.0	9.1	52.0
2.50	2.4	19.8	1.7	19.8	8.0	15.6	58.1	—	—
3.0	3.2	23.5	2.2	23.5	9.0	21.1	62.1	—	—
4.0	4.8	30.0	3.2	30.1					

λ, μ	n	ϰ	λ, μ	n	ϰ
b) Visible and near infrared regions (at T = 295°K, from [96, 119])*					
0.40	0.32	3.72	0.80	1.78	6.87
0.45	0.41	4.06	0.85	1.91	6.90
0.50	0.50	4.59	0.875	1.82	6.87
0.55	0.60	5.01	0.90	1.70	6.97
0.60	0.77	5.46	0.95	1.40	7.22
0.65	0.98	5.97	1.00	1.17	7.58
0.70	1.26	6.40	1.10	0.85	8.33
0.75	1.50	6.72	1.20	0.78	9.16

*In [96, 119], besides the directly-measured data listed in the table, there are given also the values of the optical constants obtained after taking into account the influence of the oxide film.

The optical constants of aluminum were investigated also in [70, 72, 83, 89, 104, 106–107, 110–111, 113, 117, 120–127].

Table VII. Optical constants of zinc

λ, μ	n	ϰ	λ, μ	n	ϰ
a) Infrared region (from [49]).					
1.23	1.17	4.92	5.0	3.77	26.2
1.55	0.95	7.28	6.0	5.8	31.6
2.14	1.01	10.65	7.0	7.6	36.1
2.68	1.26	13.3	8.0	9.05	40.7
3.19	1.86	16.6	10.0	15.3	47.6
4.0	2.58	21.3			

Table VII (cont'd)

ħω, ев	2nκ/λ ⊥c	2nκ/λ ∥c	ħω, ев	2nκ/λ ⊥c	2nκ/λ ∥c	ħω, ев	2nκ/λ ⊥c	2nκ/λ ∥c
b) Visible and near infrared regions (from Fig. 2 of [103]).								
2.39	24.1	11.6	1.48	55.3	22.4	1.09	—	12.5
2.07	37.4	15.3	1.44	52.9	22.0	1.04	—	12.7
1.82	44.7	19.4	1.41	45.4	20.8	1.01	—	12.1
1.69	53.3	22.5	1.36	35.3	19.9	0.96	—	12.2
1.64	54.0	22.6	1.28	21.7	18.7	0.93	—	11.4
1.59	55.3	23.0	1.20	13.6	18.0	0.86	—	8.0
1.56	57.0	23.2	1.18	—	11.5	0.81	—	7.7
1.52	57.0	22.6	1.12	—	12.1	0.78	—	7.6

Here ħω – quantum energy. The two columns of 2nκ/λ pertain to polarizations perpendicular to and parallel to the c axis. The discontinuity in the values of 2nκ/λ in the region 1.2 – 1.18 eV is connected with the change over to a different light receiver. This discontinuity does not affect the positions of the maxima of 2nκ/λ.

The optical constants of zinc were investigated also in [50, 104, 106, 108, 110–111, 113, 128–132].

Table VIII. Literature on the experimental investigation of the optical properties of certain non-transition polyvalent metals

Metals	Literature
Ga	106, 109–112, 116, 118, 133–134
Tl	116
Be	97, 121, 130, 135–136
Mg	50, 106, 110–112, 117, 121, 130, 132, 137
Cd	50, 106, 108, 110–113

consider the anisotropy of the optical constants, which appears for metals with non-cubic lattice. The study of the anisotropy of n and κ carried out at the present time by a group of physicists headed by Woodall.[50,106–112] Unfortunately, the measurements of the optical constants of the anisotropic metals, carried out by this group, pertain so far to mechanically polished samples, making it impossible to obtain the constants of the non-distorted metal.

5. DETERMINATION OF THE MICROSCOPIC CHARACTERISTICS OF A METAL FROM THE EXPERIMENTAL VALUES OF n AND κ

a) Long-Wave Region

Experiment shows that for polyvalent metals, at all temperatures, a weakly-anomalous skin effect is realized.[20,30 32,47–49,69] Therefore it is reasonable to use formulas (1.9a), (1.10a), (1.17), and (1.18) in the long-wave region of the spectrum. Taking (2.16) into account, we obtain the following formulas for the reduction of the experimental results:*

$$N = \frac{0.1115\cdot 10^{22}}{\lambda^2}\varkappa^2\frac{[1+(n^2/\varkappa^2)]^2}{1-(n^2/\varkappa^2)}\frac{1}{1-\beta_1}, \tag{5.1}$$

$$\nu = \frac{3.767\cdot 10^1}{\lambda}\frac{n/\varkappa}{1-(n^2/\varkappa^2)}\frac{1-\beta_2}{1-\beta_1}, \tag{5.2}$$

$$\beta_1 = 0.125\cdot 10^{-10}\langle v_F\rangle\varkappa\frac{[1+(n^2/\varkappa^2)][(\nu/\omega)-n/\varkappa)]}{[1-(n^2/\varkappa^2)][1+(\nu^2/\omega^2)]}, \tag{5.3}$$

$$\beta_2 = 0.06254\cdot 10^{-10}\langle v_F\rangle\varkappa\frac{1+(n^2/\varkappa^2)}{n/\varkappa}\frac{[1+(n/\varkappa)(\nu/\omega)]}{1+(\nu^2/\omega^2)}, \tag{5.4}$$

$$\frac{\langle v_F\rangle}{v_F^0} = \sqrt{\frac{N}{N_{\text{val}}}}, \tag{5.5}$$

$$\frac{S_F}{S_F^0} = \sqrt{\frac{N}{N_{\text{val}}}}. \tag{5.6}$$

Here $\omega = 1.884\times 10^{15}/\lambda$; β_1 and β_2 are the corrections connected with anomaly of the skin effect; λ is expressed in microns and the remaining quantities in cgs esu.

Formulas (5.1)–(5.6) make it possible to determine the microscopic characteristics of the investigated metals.* To this end it is necessary to know, besides the optical constants of the metals n and κ also N_{val} and v_F^0, which calls for measurements of the density of the investigated samples. We note that since the values of N_{val} and v_F are used only to determine $\langle v_F\rangle$, which enters in the formulas for β_1 and β_2, the values of N and ν are not very sensitive to N_{val} and v_F^0. Therefore the last two quantities can be determined with a lower accuracy. After the calculations are completed, it is necessary to verify the character of the skin effect. For the weakly-anomalous skin effect, β_1 and β_2, as well as the real and imaginary parts of the complex expansion parameter (1.18), should be smaller than unity.†

It was indicated above that to obtain the microscopic characteristics pertaining to the conduction electrons it is necessary to use measurements in the spectral interval in which the influence of the interband transitions on the optical properties can be neglected. The indicated interval can be determined experimentally as the interval in which the calculated values of N and ν do not depend on λ. By way of an example, Fig. 11 gives the results of the calculation of N for lead at

*In formulas (5.1) and (5.2), terms of order $|\epsilon'|^{-1}$ are neglected compared with unity. For metals in the long-wave region, this is perfectly valid, since $|\epsilon'|^{-1} \sim 10^{-3}-10^{-4}$.

*The solution of the system of equations (5.1) – (5.5) is best obtained by successive approximations, assuming in the zeroth approximation that $\beta_1 = \beta_2 = 0$.

† Usually $\beta_2 > \beta_1$, i.e., the influence of the anomaly of the skin effect on ν is much larger than the influence on N.

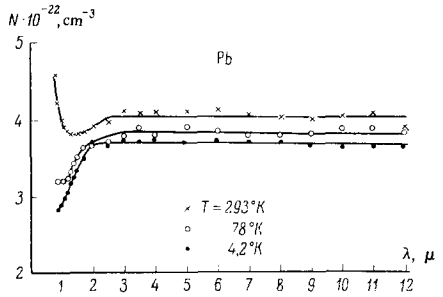

FIG. 11. Values of

$$N = \frac{0.1115\cdot 10^{22}}{\lambda^2}\,\varkappa^2\frac{(1+n^2/\varkappa^2)}{1-n^2/\varkappa^2}\,\frac{1}{1-\beta_1}$$

for different wavelengths for lead at three temperatures. In the regions 2.5–12 μ for T = 293°K, 3–12 μ for T = 78°K, and 2–12 μ for T = 4.2°K this quantity gives the concentration of the conduction electrons.

three temperatures. It is seen from the figure, that in the interval 3–12 μ the calculated values of N do not depend on λ. Consequently, measurements in this spectral interval can be used to determine the characteristics of the conduction electrons of lead.

The determination of N and ν in conjunction with measurements of the static conductivity σ_{st} and the ratio of the residual resistance to the resistance at a given temperature R_{res}/R, make it possible to calculate ν_{ep}, ν_{ep}^{cl}, ν_{ed}, l, δ and the average crystal dimension L. To this end, it is convenient to use the following relations:*

$$\left.\begin{aligned} &\nu = \nu_{ep} + \nu_{ed},\\ &\nu_{ep}^{cl} + \nu_{ed} = \frac{e^2}{m}\frac{N}{\sigma_{st}} = 2{,}533\cdot 10^8\frac{N}{\sigma_{st}} \end{aligned}\right\} \tag{5.7}$$

$$\frac{\nu_{ed}}{\nu_{ep}^{cl}+\nu_{ed}} = \frac{R_{res}}{R},$$

$$l = \frac{\langle v_F\rangle}{\nu}, \quad \delta = \frac{\lambda}{2\pi\varkappa}, \quad L = \frac{\langle v_F\rangle}{\nu_{ed}}. \tag{5.8}$$

Thus, measurements of the optical constants in the long-wave region, in conjunction with measurements of ρ, σ_{st}, and R_{res}/R make it possible to determine the following microscopic characteristics: N, $\langle v_F\rangle$, S_F, ν, ν_{ep}, ν_{ep}^{cl}, ν_{ed}, l, and δ, and also their temperature dependences.

b) Short-Wave Region

In the spectral region where an appreciable role is played both by interband and intraband transitions (these are usually the visible and near infrared regions), we use the additivity of the complex dielectric constant ϵ', i.e., we assume that

$$\varepsilon = 1 + \varepsilon_e + \tilde{\varepsilon}, \quad \sigma = \sigma_e + \tilde{\sigma}; \tag{5.9}$$

the quantities ϵ_e and σ_e pertain here to the conduction electrons and $\tilde{\epsilon}$ and $\tilde{\sigma}$ to the interband transitions.

The contribution of the conduction electrons to ϵ and σ can be determined with the aid of the microscopic characteristics obtained in the long-wave region of the spectrum, after which it is easy to determine the contribution of the interband transitions. Confining ourselves to terms of first order in β_1 and β_2, we obtain for the contribution of the conduction electrons the following formula:[20,47,48]

$$\left.\begin{aligned} &\varepsilon_e = -\left(4\pi e^2\frac{N}{m}\right)\frac{1}{\omega^2+\nu^2}(1-B_1),\\ &B_1 = \beta_1 + \frac{2\nu^2}{\omega^2+\nu^2}(\beta_2-\beta_1), \end{aligned}\right\} \tag{5.10}$$

$$\left.\begin{aligned} &\sigma_e = \left(e^2\frac{N}{m}\right)\frac{\nu}{\omega^2+\nu^2}(1-B_2),\\ &B_2 = \beta_2 + \frac{2\omega^2}{\omega^2+\nu^2}(\beta_1-\beta_2). \end{aligned}\right\} \tag{5.11}$$

Greatest interest attaches to the function $\tilde{\sigma}(\omega)$, since the positions of its maxima determine the Fourier components of the pseudopotential. The measurements at helium and nitrogen temperatures make it possible to separate $\tilde{\sigma}$ with greater accuracy than measurements at room temperature, since the contribution of the conduction electrons to σ is small at low temperatures.

For polyvalent metals in the visible and in the near infrared regions, maxima are observed on the $\tilde{\sigma}(\omega)$ curve. This makes it possible to break up $\tilde{\sigma}$ into individual bands, assuming that $\tilde{\sigma} = \sum_g \tilde{\sigma}_g$. The widths of the bands and their positions are minimal at helium temperature, increasing noticeably with increasing temperature to room temperature. Therefore the accuracy with which the bands are separated is maximal at room temperatures. Figure 12 shows by way of an example the dependence of $\tilde{\sigma}(\omega)$ of indium on $\hbar\omega$ at helium temperature. One can see clearly two maxima corresponding to the two bands of $\tilde{\sigma}_g$. Similar relations are obtained for other metals. The observed bands can usually be identified with transitions determined by different Bragg planes. In the case of anisotropic metals, it is convenient to use here measurements of $\tilde{\sigma}$ performed on single crystals in polarized light.[49,50,103] For isotropic metals or in the case of polycrystalline samples of anisotropic metals, it is possible to use the relative values of $\tilde{\sigma}_g$, and also additional information from other effects, in particular from the van Alphen–de Haas effect.[20,47-48]

The positions of the maxima and the widths of the bands of the interband conductivity make it possible to determine by means of formula (2.35) the absolute values of the Fourier components of the pseudopotential. In practice one can put $t \approx 1.05$ in this formula in the case of those bandwidths that are normally observed in the experiments.

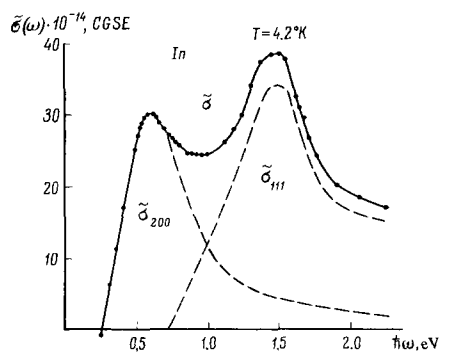

FIG. 12. Dependence of the interband conductivity $\tilde{\sigma}(\omega)$ on $\hbar\omega$ for polycrystalline indium at T = 4.2°K. ● – experimental values; – – $\tilde{\sigma}_{111}$ and $\tilde{\sigma}_{200}$.

*In (5.7) no account is taken of the frequency of the interelectron collisions ν_{ee}, since experiment shows that $\nu_{ee} \ll \nu$ [20, 30–32, 47–48].

Thus, measurements in the short-wave region make it possible to obtain the absolute values of the Fourier components of the pseudopotential $|V_g|$ and to calculate with their aid the same electronic characteristics that are determined independently from measurements in the long-wave region.

6. COMPARISON OF THE EXPERIMENTAL RESULTS WITH THE THEORY

a) Determination of the Fourier Components of the Pseudopotential by the Optical Method. Interband Transitions

It was indicated in Ch. 2 that the optical measurements in the short-wave spectral region (i.e., in the region where interband transitions are significant) make it possible to determine, from the positions of the maxima of the interband conductivity, the absolute values of the Fourier components of the pseudopotential $|V_g|$. This was performed for lead, tin, aluminum, indium, and zinc. Experimentally, V_g can be determined also from the van Alphen–de Haas effect and from cyclotron resonance. This case requires a complicated mathematical reduction of the experimental results. At the present time, such a reduction has been performed only for aluminum and lead at helium temperatures. Table IX presents a comparison of the values of $|V_g|$ for aluminum and lead, obtained by an optical method[20,46,48] and by the method of the van Alphen–de Haas effect.[51,52] The accuracies with which the larger and smaller components were determined are ~2–5% and ~5–10%, respectively. It is seen from the table that the values of $|V_g|$ obtained by both methods are in sufficiently good agreement.

Table X lists the values of $|V_g|$ determined by the optical method for certain non-transition polyvalent metals in the temperature range from room temperature to helium temperature.

The experimental and theoretical forms of the interband conductivity bands are compared in [20,46]. To this end, the aluminum band $\tilde{\sigma}_{200}$ was used, since it is sufficiently well isolated from the other bands and is located in the spectral region where the contribution of the conduction electrons to the total conductivity is small. In addition, no structure connected with the spin-orbit interaction should be observed in the aluminum bands. Comparison has shown that the experimental and theoretical forms of the bands are in sufficiently good agreement.

Table IX. Determination of the Fourier components of the pseudopotential by various methods

Metal	$\lvert V_{111}\rvert$, eV		$\lvert V_{200}\rvert$, eV	
	Optical method	From the van Alphen–de Haas effect	Optical method	From the van Alphen–de Haas effect
Al	0.22	0.24	0.72	0.76
Pb	1.11	1.14	0.70	0.53

An investigation of the dispersion of the interband conductivity makes it possible to determine, from the widths of the experimental $\tilde{\sigma}_g(\omega)$ curves, the relative broadening of the energy levels γ_g', by using the relations (2.36). Further, from (2.32)–(2.33) it is possible to calculate the absolute values of $\tilde{\sigma}_g$. A comparison of the experimental and the theoretical absolute values of $\tilde{\sigma}_g$ has shown, that the experimental values are approximately half as large as the calculated ones.* The indicated difference, apparently, is connected, first, with the fact that ΔE, which enters in formula (2.25), changes slightly[55] along the plane of the ring M_1M_2 on Fig. 2, and second, with the fact that the equality (2.25) is not satisfied in the region of the intersection of several Bragg planes.

On the whole it can be assumed that the results of an investigation of the interband conductivity confirm the assumption that the structures of the bands of the interband conductivity in the visible and in the near infrared regions of the spectrum are connected in the main with the Bragg energy splitting.

b) Determination of the Main Electronic Characteristics

We proceed to the question of determining the main electronic characteristics N, S_F, and $\langle v_F \rangle$ from the optical measurements. We have already mentioned that the indicated quantities can be obtained, first, from measurements in the long-wave region and, second, they can be calculated from formulas (2.22)–(2.22a) using the quantities $|V_g|$ listed in Table X. The results of the determination of N by two independent methods are listed in Table XI. The accuracy with which N is determined from the long-wave measurements is ~2%, and the calculation accuracy is ~10%. It is seen from the table that for polyvalent metals $N \ll N_{val}$. It is seen further that the results of the determination of N by both methods practically coincide. A certain discrepancy is observed for aluminum. The causes of this discrepancy call for a further analysis. It is quite possible that it is connected with the influence of the interaction between electrons; this influence was considered in [28–29,138–139].

The results of Table XI show that the difference between N and N_{val} is determined in the main by the Fourier components of the pseudopotential. A similar picture is obtained for S_F and $\langle v_F \rangle$. The deviation of these characteristics from the values corresponding to free electrons (at a concentration equal to the valence concentration) is also determined mainly by the Fourier components of the pseudopotential. This is seen from Tables XII and XIII.

Table XII lists also the values of S_F/S_F^0 obtained both by the optical method and by the method of investigating the anomalous skin effect in the microwave band. We see that, with the exception of aluminum, the results of both methods are in agreement (the error in the determination of S_F/S_F^0 is approximately 10%).

Let us stop to discuss the accuracy of the formulas derived in Ch. 2. To this end, we compare the results of the calculation of the ratio S_F/S_F^0 by means of for-

*Theories based on the special role of high-symmetry points give values of $\tilde{\sigma}_g$ which are smaller than the experimental ones by a factor of 5–10. [61].

Table X. Values of $|V_g|$ determined by the optical method, for certain non-transition polyvalent metals

Metal	T, °K	$\|V_1\|$, eV	$\|V_2\|$, eV	$\|V_3\|$, eV	Literature
Pb	4.2	1.11	0.70	—	20, 48
	78	1.13	0.65	—	
	293	1.17	0.51	—	
Sn	4.2	0.61	0.30	—	20
	78	0.60	0.30	—	
	293	0.57	0.22	—	
In	4.2	0.70	0.28	0.28	20, 46
	295	0.59	0.27	0.27	
Al	295	0.22	0.72	—	20, 46
Zn	293	0.74	0.50	<0.36	49

For Pb, Al, and In we have $|V_1| = |V_{111}|$ and $|V_2| = |V_{200}|$; for In – $|V_3| = |V_{002}|$; for Zn – $|V_1| = |V_{1\bar{1}0,1}|$, $|V_2| = |V_{000,2}|$, $|V_3| = |V_{1\bar{1}0,0}|$, for Sn – $|V_1| \approx |V_{101}| \approx \approx |V_{200}|$, $|V_2| \approx |V_{220}| \approx |V_{211}|$ (for Sn, the indicated identification of the Fourier components of the pseudopotential is at the present time still not unique).

Table XI. Concentration of the conduction electrons N, obtained from measurements in the long-wave region and calculated from the values of the Fourier components of the pseudopotential $|V_g|$

Metal	T, °K	N/N_a from long-wave measurements	N/N_a from $\|V_g\|$	N_{val}/N_a	Literature
Pb	4.2	1.11	1.13	4	20, 48
	78	1.15	1.13		
	293	1.23	1.25		
Sn	4.2	1.12	0.96	4	20
	78	1.12	0.99		
	293	1.30	1.41		
In	4.2	1.42	1.52	3	20, 47
	295	1.76	1.70		
Al	78	1.25	—	3	20, 43
	295	1.31	2.02		
Zn	293	0.51	<0.79	2	49

mulas (2.14), based on the solution of a second-order secular equation, with the calculation of this quantity based on the solution of a fourth-order secular equation. The latter calculation was performed for lead in [52]. Using the values V_{111} and V_{200}, determined from the van Alphen–de Haas effect (see Table IX), we obtain $S_F/S_F^0 = 0.589$ in accordance with [52] and 0.638 in accordance with formulas (2.14). Further, for the density of the electronic states on the Fermi surface* we obtain $(dY/dE)_F/(dY/dE)_{0F} = 1$ using a second-order secular equation and 0.87 (for lead) using a fourth-order secular equation.[52] It can thus be assumed that the error in the formulas of Ch. 2 is approximately 10%.

Tables XII and XIII make it also possible to estimate the accuracy of the approximate formulas (2.16). Comparing the data of the third and fourth columns, we find that the error in the approximate formulas is also of the order of 10%.

c) Temperature Dependence of the Electronic Characteristics

The optical method is at present the only one that makes it possible to obtain the temperature dependence of $|V_g|$, N, S_F, and $\langle v_F \rangle$ in a wide temperature range. This temperature dependence is given in Tables X–XIII. When the temperature increases from that in liquid helium to room temperature, $|V_g|$ of the investigated metals drop by approximately 4–25% (with the exception of $|V_{111}|$ for lead, which increases by about 6%), N increase by about 5–25%, and S_F and $\langle v_F \rangle$ increase by approximately 3–12%. Figure 13 shows by way of an example the N(T) dependence observed for all the investigated metals. The increase of N on going from nitrogen temperature to room temperature is larger than on going from helium temperature to nitrogen temperature. Above room temperature, the N(T) dependence should be even stronger. This conclusion is in qualitative agreement with the results of the determination of the optical constants of tungsten at high temperatures.[145]

Table XII. Values of S_F/S_F^0 calculated from $|V_g|$ and measured by the optical method and by the microwave method

Metal	T°, K	По $\|V_g\|$: From formula (2,14)	По $\|V_g\|$: From formula (2,16)	Optical measurements: S_F/S_F^0	Optical measurements: Reference	Measurements in the microwave band: S_F/S_F^0	Measurements in the microwave band: Reference
Pb	4.2	0.61	0.53	0.53	20, 48	0.55	140
	78	0.61	0.53	0.54		—	
	293	0.62	0.56	0.56		—	
Sn	4.2	—	0.49	0.53	20	0.55	141
	78	—	0.50	0.53		—	
	293	—	0.59	0.57		—	
In	4.2	0.72	0.71	0.69	20, 47	—	—
	295	0.77	0.75	0.77		—	
Al	78	—	—	0.64	20	1.0	141
	295	0.81	0.82	0.66		—	
Zn	295	—	—	0.50	49	0.41	141

*The experimental determination of the density of states of the electrons on the Fermi surface with the aid of the electronic specific heat includes the phonon "overgrowth" considered in [142, 143]. This phonon "overgrowth" does not come into play in optics [144].

Table XIII. Values of $\langle v_F \rangle \times 10^8$ (cm/sec) calculated from $|V_g|$ and measured by the optical method

Metal	T, °K	По $\|V_g\|$: From formula (2,15)	По $\|V_g\|$: From formula (2,16)	Optical measurements	Reference	$v_F^0 \cdot 10^8$
Pb	4.2	0.85	0.97	0.97	20, 48	1.84
	78	0.85	0.97	0.98		1.83
	293	0.92	0.92	1.01		1.82
Sn	4.2	—	0.93	1.00	20	—
	78	—	0.94	1.00		—
	293	—	1.12	1.08		1.89
In	4.2	1.22	1.24	1.20	20, 47	—
	295	1.29	1.31	1.34		1.74
Al	78	—	—	1.30	20	—
	295	1.67	1.65	1.33		2.02
Zn	293	—	—	0.92	49	1.82

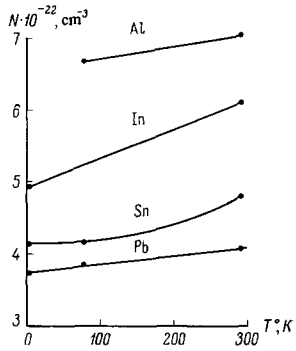

FIG. 13. Temperature dependence of the conduction electron concentration, obtained from measurements in the long-wave region.

Table XIV. N(T) dependence for Al and Pb, obtained by optical and x-ray methods

Metals	$N(T_R)/N(T_N)$: "Optics"	$N(T_R)/N(T_N)$: "X-ray"
Al	1.05	1.04
Pb	1.07	1.11

Unfortunately, the optical constants were determined in that reference only for the near infrared region, where the contribution from the interband transitions may be appreciable.

It follows from Table XI that the temperature dependence of N is determined by the temperature dependence of $|V_g|$.

It was shown in Ch. 2 that the N(T) dependence, as well as the temperature changes of the intensity of the diffraction maxima in the x-ray band, are determined by the Debye-Waller factor. Using the results of [146], in which the Debye-Waller factor was determined for the cubic metals Al and Pb from x-ray measurements, the temperature dependence of N was calculated for these metals in [20,44].* A comparison of the results of the calculation of the ratio $N(T_r)/N(T_N)$ from x-ray data with the results of the optical experiments is found in Table XIV. (Here T_r and T_N are the room and nitrogen temperatures, respectively). We see that the values of the ratio obtained by different methods are in good agreement.

Thus, the temperature dependence of the electronic characteristics agrees with the theory.

d) Collision Frequencies of Conduction Electrons and of Electrons Taking Part in the Interband Transitions

Optical measurements in the long-wave region make it possible to obtain the effective electron collision frequency ν. If the static conductivity and the ratio of the residual resistance to the resistance at a given temperature are measured simultaneously with the optical measurements, then it is possible to determine ν_{ep} and ν_{ed} (see Ch. V). The results of the determination of ν and ν_{ep} for certain metals are listed in Table XV.

Table XV. Collision frequencies of conduction electrons and of electrons taking part in the interband transitions

Metal	T, °K	Conduction electrons: $\nu \cdot 10^{-14}$	Conduction electrons: $\nu_{ep} \cdot 10^{-14}$	Conduction electrons: Reference	Electrons taking part in interband transitions: $\nu_{111} \cdot 10^{-14}$	Electrons taking part in interband transitions: $\nu_{200} \cdot 10^{-14}$	Electrons taking part in interband transitions: Reference
Pb	4.2	0.41	0.40	20, 48	7	8	20, 48
	78	0.87	0.86		10	8	
	293	3.07	3.06		15	8	
Sn	4.2	0.53	0.48	20	4 *)	—	20
	78	0.77	0.72		6 *)	—	
	293	2.27	2.21		9 *)	—	
In	4.2	0.58	0.54	20, 47	7	4	20, 46
	295	2.24	2.19		8	6	
Al	78	0.72	—	20	—	—	20, 46
	295	1.21	1.05		—	2	
Zn	293	1.08	—	49	—	—	—

ν, ν_{ep}, ν_{111} and ν_{200} — в sec^{-1}.

*The values given for tin are those pertaining to the band V_1.

Optical measurements in the short-wave region make it possible to determine, the broadening of the energy levels from the width of the $\tilde{\sigma}_g(\omega)$ bands, and to estimate, by using the uncertainty relation, the effective collision frequency ν_g for the electrons taking part in the interband transitions near the Bragg plane g (see Ch. II). The results of the determination of ν_{111} and ν_{200} are also listed in Table XV for a number of metals.

*No account was taken in [44] of the temperature dependence of the lattice constant. This dependence was taken into account in [20] and in the present paper.

A comparison of ν with ν_g shows that $\nu_g > \nu$. The temperature dependence of ν_g is much weaker than the temperature dependence of ν, and accordingly at low temperatures $\nu_g \gg \nu$.

The short lifetimes of the electrons taking part in the interband transitions may be due to the strong interelectron interaction. This interaction is larger than the corresponding interaction for an electron on the Fermi surface, since the energies of the ground and excited states differ from the Fermi energy by an amount greatly exceeding kT. The interelectron interaction can lead to the collective Auger effect indicated in [61,147], which also reduces the lifetime of the excited state.

Let us examine the temperature dependence of the electron-phonon collision frequency ν_{ep}, which determines the optical properties of metals. This temperature dependence is much weaker than the temperature dependence of the analogous frequency ν_{ep}^{cl}, which enters in the static electric conductivity. The reason is the quantum character of the interaction of the electron with the photon and with the phonons. This question is considered theoretically in [10-12].

At high temperatures, when $T > \Theta_R$ and there are many phonons, the interaction of the electrons with the phonons, both in optics and in statics, leads to approximately the same collision frequency, i.e., $\nu_{ep} \approx \nu_{ep}^{cl}$ at $T > \Theta_R$. Here Θ_R is the characteristic temperature, obtained from the temperature dependence of the resistance. It is close to the Debye temperature. At low temperatures $T \ll \Theta_R$ there are few phonons, especially high-energy ones. Therefore, in static phenomena, the electron is practically unable to absorb high-energy phonons. Nor does the electron have enough energy to emit such phonons. As a result, we get $\nu_{ep}^{cl}(T) \sim T^5$ when $T \ll \Theta_R$.

In optics, an electron absorbing a quantum of light is ejected far beyond the Fermi-surface smearing level. In this case it cannot absorb high-energy phonons, of which there are none, but it can emit the entire phonon spectrum. This leads to a large collision frequency. According to [10-12], $\nu_{ep}(T) \to 0.4\,\nu_\Theta$ when $T \ll \Theta_R$; here $\nu_\Theta = 0.94\,\nu_{ep}(\Theta_R)$.

Figure 14 shows theoretical plots of ν_{ep}/ν_Θ and ν_{ep}^{cl}/ν_Θ on T/Θ_R, obtained in [11]. The figure shows the large discrepancy between these curves when T is close to zero.

The experimental temperature dependence $\nu_{ep}(T)$ is given in Table XV. The main qualitative effect is seen immediately. Even at helium temperatures, ν_{ep} remains a large quantity, equal to $(4-5)\times 10^{13}$ sec^{-1}. For comparison we indicate that for gold at room temperature $\nu_{ep} = 4\times 10^{13}$ sec^{-1}. The ratio ν_{ep}/ν_{ep}^{cl} at helium temperature for the investigated metals is equal to 10^4–10^6.

To compare the theoretical and experimental temperature dependences, it is best to consider the ratios of the frequencies ν_{ep} pertaining to different temperatures. In this case all the coefficients, which are theoretically determined with low accuracy, drop out. The comparison shows that the theory yields the correct temperature dependence of $\nu_{ep}(T)$. This is clearly seen from Fig. 14, which shows besides the theoretical curve also the experimental dependence of ν_{ep}/ν_Θ on T/Θ_R for Pb, Sn, and In.[20,31-32,36,47] The value of Θ_R was determined from the temperature dependence of the static

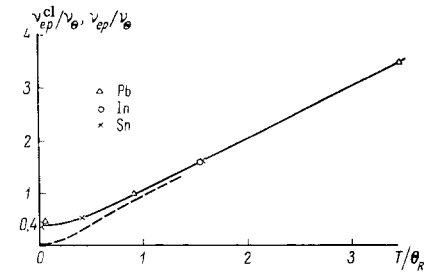

FIG. 14. Experimental and theoretical dependences of the electron-phonon collision frequencies on the reduced temperature. Solid curve—theoretical dependence of $\nu_{ep}(T)/\nu_\Theta$ on T/Θ_R; dashed —theoretical dependence of $\nu_{ep}^{cl}(T)/\nu_\Theta$ on T/Θ_R; the experimental values of $\nu_{ep}(T)/\nu_\Theta$ for indium, tin, and lead.

conductivity. It turned out to be equal to 85° K for Pb, 187° K for Sn, and 190° K for In. The coefficient ν_Θ was determined by aligning the experimental values pertaining to the room temperature with the theoretical curve. It turned out here that $\nu_{ep}(T_N)/\nu_\Theta$ and $\nu_{ep}(T_{He})/\nu_\Theta$ fit the curve quite well (here $T_N = 78°$ K and $T_{He} = 4.2°$ K). In particular, the mean value of $\nu(T_{He})/\nu_\Theta$ for the three indicated metals turned out to be 0.42, which is in good agreement with the theoretical value 0.40. Thus, theory yields the correct temperature dependence of $\nu_{ep}(T)$.

The experimental data given in [20,47,48] make it also possible to compare the experimental and theoretical absolute values of ν_{ep}. According to the theory, $\nu_{ep} \approx \nu_{ep}^{cl}$ when $T > \Theta_R$. For lead, tin, and indium $T_r > \Theta_R$ (here T_r is the room temperature), but ν_{ep} is approximately 30% larger than ν_{ep}^{cl}.

Thus, the absolute values of ν_{ep}, obtained from experiment, are approximately 30% larger than the theoretical ones. The reason may be that the theory does not take accurate account of the high-frequency acoustic and optical oscillations.

7. CONCLUSION

On the whole, it can be assumed that the experiments confirm the theory presented in the present article. The optical properties of non-transition metals in the infrared and visible parts of the spectrum can be successfully described by the weak-coupling scheme. The difference between the characteristics of the conduction electrons, which determine the optical properties in the infrared region of the spectrum, and the characteristics of the free electrons is determined principally by the Fourier components of the pseudopotential, corresponding to Bragg planes intersecting the free-electron sphere. The optical properties in the visible and in the near infrared regions of the spectrum are determined principally by the interband transitions connected with the Bragg energy splitting. The electronic characteristics obtained from measurements in both indicated regions of the spectrum are in good agreement with each other.

Metal optics makes it possible to obtain a number of fundamental electronic characteristics of metals: the concentration of the conduction electrons, the average velocity of the electrons on the Fermi surface, the total area of the Fermi surface, the Fourier components of the pseudopotential, and the effective electron collision frequencies. The results obtained by the optical method

are in good agreement with the analogous results obtained from other effects. However, metal optics, compared with other effects, gives the largest assortment of microscopic characteristics. In addition, at the present time only optics yields the temperature dependence of the indicated characteristics. We can hope that further development of metal-optic investigations will further increase their role in the development of metal physics.

LIST OF SYMBOLS

$\epsilon' \equiv \epsilon - i\epsilon \equiv \epsilon - i\frac{4\pi}{\omega}\sigma \equiv (n - i\kappa)^2$ — Complex dielectric constant;

$n - i\kappa$ — complex refractive index;

$\epsilon_1 = \mathrm{Re}\,\epsilon'$, $\epsilon_2 = -\mathrm{Im}\,\epsilon'$;

ϵ — dielectric constant;

ϵ_e — contribution made to the dielectric constant by the conduction electrons;

$\tilde{\epsilon}$ — contribution made to the dielectric constant by the electrons taking part in the interband transitions;

σ — conductivity;

σ_e — contribution of conduction electrons to the conductivity;

$\tilde{\sigma}$ — contribution of the electrons taking part in the interband transitions to the conductivity;

$\mathscr{E}$ — electric field of light wave;

λ — wavelength of light; ω — cyclic frequency of light; c — velocity of light;

$\tilde{f} = f_0 + f$ — electron distribution function; f_0 — equilibrium electron distribution function;

f — nonequilibrium addition to the electron distribution function;

j — current density;

E — electron energy;

E_F — Fermi energy;

E_F^0 — Fermi energy for free electrons at a concentration N_{val};

m — mass of free electrons;

e — electron charge;

N — conduction-electron concentration;

N_{val} — valence electron concentration;

N_a — atom concentration;

p — electron momentum;

p_F^0 — Fermi momentum for free electrons at concentration N_{val};

$\mathscr{K}$ — wave vector of electron;

v — electron velocity;

$\langle v_F \rangle$ — average electron velocity on the Fermi surface;

v_F^0 — velocity of free electrons on the Fermi surface at concentration N_{val};

S_F — total area of the Fermi surface in momentum space;

S_F^0 — area of Fermi surface for the free electrons at concentration N_{val};

ν — effective electron collision frequency;

ν_{ep} — electron-phonon collision frequency;

ν_{ep}^{cl} — classical electron-phonon collision frequency;

ν_{ee} — interelectron collision frequency;

ν_{ed} — frequency of collisions between the electron and impurities or defects;

l — mean free path of electron;

$\delta = \lambda/(2\pi\kappa)$ — skin-layer depth;

T — absolute temperature;

k — Boltzmann's constant;

V — pseudopotential;

V_g — Fourier component of pseudopotential;

g — reciprocal-lattice vector;

a — lattice period for cubic systems.

[1] V. L. Ginzburg and G. P. Motulevich, Usp. Fiz. Nauk **55**, 469 (1955); Fortschr. d. Phys. **3**, 309 (1955).

[2] R. B. Dingle, Physica **19**, 312, 348, 729 (1953).

[3] V. L. Ginzburg, Dokl. Akad. Nauk SSSR **97**, 999 (1954).

[4] A. B. Pippard, Proc. Roy. Soc. **A191**, 385 (1947).

[5] G. E. Reuter and E. H. Sondheimer, Proc. Roy. Soc. **A195**, 336 (1949).

[6] R. G. Chambers, Nature **165**, 239 (1950); Proc. Roy. Soc. **215**, 481 (1952).

[7] T. Holstein, Phys. Rev. **88**, 1427 (1952).

[8] P. Drude, Wied. Ann. **32**, 584 (1887); **36**, 532 (1889); **39**, 481, 507 (1890); Lehrbuch der Optik, Leipzig, 1900. C. Zener, Nature **132**, 968 (1933).

[9] Manfred A. Biondi, Phys. Rev. **96**, 534 (1954).

[10] R. N. Gurzhi, Zh. Eksp. Teor. Fiz. **33**, 451, 660 (1957) [Sov. Phys.-JETP **6**, 352 (1958)].

[11] R. N. Gurzhi, Dissertation, FTI, AN USSR, Khar'kov, 1958.

[12] T. Holstein, Phys. Rev. **96**, 535 (1954).

[13] W. A. Harrison, Phys. Rev. **118**, 1182, 1190 (1962); **126**, 497 (1962); **129**, 2503, 2512 (1963).

[14] V. Heine, Low Temperature Physics LT9, part B, Plenum Press, New York, 1964, p. 698.

[15] V. Heine, Optical Properties and Electronic Structure of Metals and Alloys. Proc. of the 1-st Intern. Coll., Paris, 1965, F. Abelés Ed., North-Holland Publishing Co., Amsterdam, 1966, p. 16.

[16] J. M. Ziman, Electrons and Phonons, Oxford, 1960.

[17] J. M. Ziman, Contemporary Physics **3**, 401 (1962).

[18] J. M. Ziman, Advances in Phys. **13**, 89 (1964).

[19] J. M. Ziman, Theory of Solids, Cambridge Univ. Press.

[20] G. P. Motulevich, Doctoral Dissertation, FIAN, 1968.

[21] H. Bethe and A. Sommerfeld, Electron Theory of Metals (Russ. Transl.) ONTI, 1938.

[22] A. H. Wilson, Theory of Metals, Cambridge, 1936.

[23] E. H. Sondheimer, Adv. in Phys. **1**, 1 (1952).

[24] M. Ya. Azbel' and É. A. Kaner, Zh. Eksp. Teor. Fiz. **32**, 896 (1957) [Sov. Phys.-JETP **5**, 730 (1957)].

[25] N. N. Bogolyubov and K. P. Gurov, Zh. Eksp. Teor. Fiz. **17**, 614 (1947).

[26] Yu. P. Klimontovich and V. P. Silin, Zh. Eksp. Teor. Fiz. **23**, 151 (1952).

[27] V. L. Ginzburg and V. P. Silin, Zh. Eksp. Teor. Fiz. **29**, 64 (1955) [Sov. Phys.-JETP **2**, 46 (1956)].

[28] L. P. Pitaevskiĭ, Zh. Eksp. Teor. Fiz. **34**, 942 (1958) [Sov. Phys.-JETP **7**, 652 (1958)].

[29] R. N. Gurzhi, Zh. Eksp. Teor. Fiz. **35**, 965 (1958) [Sov. Phys.-JETP **8**, 673 (1959)].

[30] A. I. Golovashkin and G. P. Motulevich, Zh. Eksp. Teor. Fiz. **44**, 398 (1963) [Sov. Phys.-JETP **17**, 271 (1963)].

[31] A. I. Golovashkin, Zh. Eksp. Teor. Fiz. 48, 825 (1965) [Sov. Phys.-JETP 21, 548 (1965)].
[32] A. I. Golovashkin, Trudy FIAN 39, 91 (1967).
[33] R. B. Dingle, Appl. Sci. Res. B3, 69 (1953).
[34] A. N. Gordon and E. H. Sondheimer, Appl. Sci. Res. B3, 297 (1953).
[35] A. V. Sokolov, Opticheskie svoĭstva metallov (Optical Properties of Metals), Fizmatgiz, 1961.
[36] A. I. Golovashkin and G. P. Motulevich, Zh. Eksp. Teor. Fiz. 47, 64 (1964) [Sov. Phys.-JETP 20, 44 (1965)].
[37] Ya. L. Al'pert, V. L. Ginzburg, and E. L. Feĭnberg, Rasprostranenie radiovoln (Radio Wave Propagation), Gostekhizdat, 1953.
[38] G. P. Motulevich, Zh. Eksp. Teor. Fiz. 37, 1770 (1959) [Sov. Phys.-JETP 10, 1249 (1960)].
[39] S. V. Vonsovskiĭ, Izv. AN SSSR, ser. fiz. 12, 337 (1948); Usp. Fiz. Nauk 48, 289 (1952).
[40] G. P. Motulevich and A. A. Shubin, Zh. Eksp. Teor. Fiz. 44, 48 (1963) [Sov. Phys.-JETP 17, 33 (1963)].
[41] G. P. Motulevich, Zh. Eksp. Teor. Fiz. 46, 287 (1964) [Sov. Phys.-JETP 19, 199 (1964)].
[42] M. I. Kaganov and V. V. Slezov, Zh. Eksp. Teor. Fiz. 32, 1496 (1957) [Sov. Phys.-JETP 5, 1216 (1957)].
[43] R. N. Gurzhi and G. P. Motulevich, Zh. Eksp. Teor. Fiz. 51, 1220 (1966) [Sov. Phys.-JETP 24, 818 (1967)].
[44] G. P. Motulevich, Zh. Eksp. Teor. Fiz. 51, 1918 (1966) [Sov. Phys.-JETP 24, 1287 (1967)].
[45] A. I. Golovashkin, A. I. Kopeliovich, and G. P. Motulevich, ZhETF Pis. Red. 6, 651 (1967) [JETP Lett. 6, 142 (1967)].
[46] A. I. Golovashkin, A. I. Kopeliovich, and G. P. Motulevich, Zh. Eksp. Teor. Fiz. 53, 2053 (1967) [Sov. Phys.-JETP 26, 1161 (1968)].
[47] A. I. Golovashkin, I. S. Levchenko, G. P. Motulevich, and A. A. Shubin, Zh. Eksp. Teor. Fiz. 51, 1622 (1966) [Sov. Phys.-JETP 24, 1093 (1967)].
[48] A. I. Golovashkin and G. P. Motulevich, Zh. Eksp. Teor. Fiz. 53, 1526 (1967) [Sov. Phys.-JETP 26, 881 (1968).
[49] G. P. Motulevich and A. A. Shubin, Zh. Eksp. Teor. Fiz. 56, 45 (1969) [Sov. Phys.-JETP 29, 24 (1969)].
[50] R. H. W. Graves and A. P. Lenham, J. Opt. Soc. Am. 58, 126 (1968).
[51] N. W. Ashcroft, Phil. Mag. 8, 2055 (1963).
[52] J. R. Anderson and A. V. Gold, Phys. Rev. 139, A1459 (1965).
[53] A. I. Ansel'm, Vvedenie v teoriyu poluprovodnikov (Introduction to Semiconductor Theory), Fizmatgiz, 1965.
[54] E. Jahnke and F. Emde, Tables of Functions, Dover, 1943.
[55] W. A. Harrison, Phys. Rev. 147, 467 (1966).
[56] M. I. Sergeiev and M. G. Tchernikhovsky, Phys. Zs. Sowietunion 5, 106 (1934).
[57] L. D. Landau and E. M. Lifshitz, Kvantovaya mekhanika, Fizmatgiz, 1963 (Quantum Mechanics, Addison-Wesley, 1965); W. Heitler, The Quantum Theory of Radiation, Oxford, 1953.
[58] Van Hove, Phys. Rev. 89, 1189 (1953).
[59] J. C. Phillips, Phys. Rev. 104, 1263 (1956).
[60] J. C. Phillips. J. Phys. Chem. Solids 12, 208 (1960).
[61] J. C. Phillips, Optical Properties and Electronic Structure of Metals and Alloys. Proc. of the 1st Intern. Coll., Paris, 1965, F. Abelés Ed., North-Holland Publishing Co., Amsterdam, 1966, p. 22.
[62] D. Brust, Y. C. Phillips, and F. Bassani, Phys. Rev. Lett. 9, 94 (1962).
[63] W. Kohn, Optical Properties and Electronic Structure of Metals and Alloys. Proc. of the 1-st Intern. Coll., Paris, 1965, F. Abelés Ed., North-Holland Publishing Co., Amsterdam, 1966, p. 1.
[64] R. W. James, Optical Principles of the Diffraction of X Rays, Cornell, 1948.
[65] P. Debye, Ann. der Phys. 43, 49 (1914). I. Waller, Zs. f. Phys. 17, 398 (1923).
[66] L. I. Mirkind, Spravochnik po rentgenostrukturnomy analizy polikristallov (Handbook of X-ray Structure Analysis of Polycrystals), Fizmatgiz, 1961.
[67] G. P. Motulevich and A. A. Shubin, Opt. Spektrosk. 2, 633 (1957); Materialy X Vsesoyuznogo soveshchaniya po spektroskopii (Proc. Tenth All-union Conf. on Spectroscopy) 1, 95 (1957).
[68] A. I. Golovashkin, G. P. Motulevich, and A. A. Shubin, PTÉ No. 5, 74 (1960).
[69] A. I. Golovashkin and G. P. Motulevich, Zh. Eksp. Teor. Fiz. 46, 460 (1964) [Sov. Phys.-JETP 19, 310 (1964)].
[70] I. N. Shklyarevskiĭ and V. K. Miloslavskiĭ, Opt. Spektrosk. 3, 361 (1957).
[71] I. N. Shklyarevskiĭ, N. G. Starunov, and V. G. Padalka, Opt. Spektrosk. 4, 792 (1958).
[72] J. R. Beattie, Phil. Mag. 46, 235 (1955); Physica 23, 898 (1957).
[73] M. M. Noskov and B. A. Charikov, Opt. Spektrosk. 1, 1007 (1956).
[74] H. Bode, Network Analysis and Feedback Amplifier Design, New Jersey, 1945.
[75] D. E. Thomas, Bell System Tech. J. 26, 870 (1947).
[76] T. S. Robinson, Proc. Phys. Soc. (London) 65, 910 (1952).
[77] F. C. Yahoda, Phys. Rev. 107, 1261 (1957).
[78] H. R. Philipp and E. A. Taft, Phys. Rev. 113, 1002 (1959).
[79] F. Stern, Solid State Physics 15, 299 (1963).
[80] L. D. Landau and E. M. Lifshitz, Élektrodinamika sploshnykh sred, Gostekhizdat, 1957, p. 324 (Electrodynamics of continuous media, Addison-Wesley, 1959).
[81] E. A. Taft and H. R. Philipp, Phys. Rev. 121, 1100 (1961).
[82] H. Ehrenreich and H. R. Philipp, Phys. Rev. 128, 1622 (1962).
[83] H. Ehrenreich, H. R. Philipp, and B. Segall, Phys. Rev. 132, 1918 (1963).
[84] B. R. Cooper, H. Ehrenreich, and H. R. Philipp, Phys. Rev. 138, A494 (1965).
[85] M. M. Kirillova and B. A. Charikov, FMM 19, 495 (1965).
[86] M. M. Kirillova, L. V. Nomerovannaya, G. A. Bolotin, V. M. Maevskiĭ, M. M. Noskov, and M. S. Bolotina, FMM 25, 459 (1968).
[87] V. K. Miloslavskiĭ, Soobshchenie na Ukrainskoĭ respublikanskoĭ konferentsii po molekulyarnoĭ spektroskopii (Report at Ukrainian Republic Conference on Molecular Spectroscopy), L'vov, 1966.
[88] M. P. Givens, Solid State Physics 6, 313 (1957).
[89] L. G. Schulz, Adv. Phys. 6, 102 (1957).
[90] A. I. Golovashkin, G. P. Motulevich, and A. A. Shu-

bin, Zh. Eksp. Teor. Fiz. 38, 51 (1960) [Sov. Phys.-JETP 11, 38 (1960)].
[91] G. P. Motulevich and A. A. Shubin, Zh. Eksp. Teor. Fiz. 47, 840 (1964) [Sov. Phys.-JETP 20, 560 (1965)].
[92] K. V. Bol'shova, I. S. Levchenko, and A. A. Shubin, PTÉ 228 (1968).
[93] A. I. Golovashkin, I. E. Leksina, G. P. Motulevich, and A. A. Shubin, Zh. Eksp. Teor. Fiz. 56, 51 (1969) (Sov. Phys.-JETP 29, 27 (1969)].
[94] I. E. Leksina, G. P. Motulevich, L. N. Fedotov, and A. A. Shubin, FMM 23, 511 (1967).
[95] L. A. Ageev and I. N. Shklyarevskiĭ, Fiz. Tverd. Tela 9, 2958 (1967) [Sov. Phys.-Solid State 9, 2324 (1968)].
[96] I. N. Shklyarevskiĭ and R. G. Yarovaya, Opt. Spektrosk. 16, 85 (1964).
[97] R. G. Yarovaya, Dissertation, Khar'kovskii Gos. Universitet, 1965.
[98] I. N. Shklyarevskiĭ, V. P. Kostyuk, and V. R. Karas', Opt. Spektrosk. 23, 147 (1967).
[99] M. Suffczynski, Physica Status Solidi 4, 3 (1964).
[100] D. Beaglehole, Optical Properties and Electronic Structure of Metals and Alloys. Proc. of the 1-st Intern. Coll., Paris, 1965, F. Abelés Ed., North-Holland Publishing Co., Amsterdam, 1966, p. 154.
[101] H. Mayer and B. Hietel, Optical Properties and Electronic Structure of Metals and Alloys. Proc. of the 1-st Intern. Coll., Paris, 1965, F. Abelés Ed., North-Holland Publishing Co., Amsterdam, 1966, p. 47.
[102] P. Erochin, Ann. der Phys. 39, 213 (1912).
[103] A. H. Lettington, Optical Properties and Electronic Structure of Metals and Alloys. Proc. of the 1-st Intern. Coll., Paris. 1965, F. Abelés Ed., North-Holland Publishing Co., Amsterdam, 1966, p. 147.
[104] J. N. Hodgson, Proc. Phys. Soc. B68, 593 (1955).
[105] J. N. Hodgson, Phil. Mag. 4, 183 (1959); 5, 272 (1960); 6, 509 (1961); 7, 229 (1962).
[106] A. P. Lenham, D. M. Treherne, and A. J. Woodall, Optical Properties and Electronic Structure of Metals and Alloys. Proc. of the 1-st Intern. Coll., Paris, 1965, F. Abelés Ed., North-Holland Publishing Co., Amsterdam, 1966, p. 40.
[107] A. P. Lenham and D. M. Treherne, Proc. Phys. Soc. 85, 167 (1965).
[108] A. P. Lenham and D. M. Treherne, Proc. Phys. Soc. 83, 1059 (1964).
[109] A. P. Lenham, Proc. Phys. Soc. 82, 933 (1963).
[110] A. P. Lenham and D. M. Treherne, J. Opt. Soc. Am. 56, 752 (1966).
[111] A. P. Lenham and D. M. Treherne, J. Opt. Soc. Am. 56, 1076 (1966).
[112] A. P. Lenham and D. M. Treherne, J. Opt. Soc. Am. 57, 476 (1967).
[113] P. Drude, Wied. Ann. 39, 481 (1890).
[114] R. Haensel, C. Kunz. T. Sasaki, and B. Sonntag, Applied Optics 7, 301 (1968).
[115] I. N. Shklyarevskiĭ and N. A. Nosulenko, Opt. Spektrosk. 2, 658 (1957).
[116] J. Bor and C. Bartholomew, Proc. Phys. Soc. 90, 1153 (1967).
[117] W. R. Hunter, J. Opt. Soc. Am. 54, 208 (1964).
[118] C. Wesolowska, E. Dobierzewska-Mozrzymasowa, and B. Jakubowski, Acta Phys. Polon. 25, 443 (1964).
[119] I. N. Shklyarevskiĭ and R. G. Yarovaya, Opt. Spektrosk. 14, 252 (1963).
[120] G. Hass and J. E. Waylonis, J. Opt. Soc. Am. 51, 719 (1961).
[121] H. M. O'Bryan, J. Opt. Soc. Am. 26, 122 (1936).
[122] L. G. Schulz, J. Opt. Soc. Am. 44, 357 (1954).
[123] L. G. Schulz and F. K. Tangherlini, J. Opt. Soc. Am. 44, 362 (1954).
[124] P.H. Berning, G. Hass, and R. P. Madden, J. Opt. Soc. Am. 50, 586 (1960).
[125] H. E. Bennett, M. Silver, and J. Ashley, J. Opt. Soc. Am. 53, 1089 (1963).
[126] H. E. Bennett and J. M. Bennett, Optical Properties and Electronic Structure of Metals and Alloys. Proc. of the 1st Intern. Coll., Paris, 1965, F. Abelés Ed., North-Holland Publishing Co., Amsterdam, 1966, p. 175.
[127] Robert La Villa and H. Mendlowitz, Phys. Rev. Lett 9, 149 (1962).
[128] W. Meier, Ann. der Phys. 31, 1017 (1910).
[129] E. I. Domanskiĭ, and M. M. Noskov, FMM 1, 567 (1955).
[130] R. O. Bock, Phys. Rev. 68, 210 (1945).
[131] J. Bor, A. Hobson, and C. Wood, Proc. Phys. Soc. 51, 932 (1939).
[132] M. E. Graber, Phys. Rev. 26, 380 (1925).
[133] A. Yu. Eĭchis and G. P. Skornyakov, Opt. Spektrosk. 16, 159 (1964).
[134] C. Wesolowska, Acta Phys. Polon. 25, 323 (1964).
[135] I. N. Shklyarevskiĭ and R. G. Yarovaya, Opt. Spektrosk. 11, 661 (1961).
[136] M. P. Givens, Phys. Rev. 61, 626 (1942).
[137] Marcel Priol, André Doudé et Simone Robin, C. R. Acad. Sc., Paris, 264, 935, 1967.
[138] V. P. Silin, Zh. Eksp. Teor. Fiz. 33, 1282 (1957) and 34, 707 (1958) [Sov. Phys.-JETP 6, 985 (1958) and 7, 486 (1958)].
[139] V. L. Ginzburg, G. P. Motulevich, and L. P. Pitaevskiĭ, Dokl. Akad. Nauk SSSR 163, 1352 (1965) [Sov. Phys.-Dokl. 10, 765 (1966)].
[140] J. E. Aubrey, Phil. Mag. 5, 1001 (1960).
[141] E. Fawcett, The Fermi Surface, Proc. of an Int. Conf., W. A. Harrison and M. B. Webb Ed., John Wiley, Sons, New York, London, 1960, p. 198.
[142] A. B. Migdal, Zh. Eksp. Teor. Fiz. 34, 1438 (1958) [Sov. Phys.-JETP 7, 996 (1958)].
[143] A. A. Abrikosov, L. P. Gor'kov, and I. E. Dzyaloshinskiĭ, Metody kvantovoĭ teorii polya v statisticheskoĭ fizike (Quantum Field Theoretical Methods in Statistical Physics), Fizmatgiz, 1962 [Pergamon, 1965].
[144] Sh. M. Kogan, Fiz. Tverd. Tela 9, 1510 (1967) [Sov. Phys.-Solid State 9, 1180 (1967)].
[145] W. S. Martin, E. H. Duchane, and H. H. Blay, J. Opt. Soc. Am. 55, 1623 (1965).
[146] D. R. Chipman, J. Appl. Phys. 31, 2012 (1960).
[147] P. Nozieres, Optical Properties and Electronic Structure of Metals and Alloys. Proc. of the 1st Intern. Coll., Paris, 1965, F. Abelés Ed., North-Holland Publishing Co., Amsterdam, 1966, p. 363.

Translated by J. G. Adashko